國　立　交　通　大　學

電信工程學系碩士班

碩士論文

IEEE 802.16 OFDMA 低複雜度內接收機設計

Low-Complexity Inner Receiver Design for IEEE 802.16 OFDMA Systems

研 究 生：丁偉家　　Student：Wei-Chia Ting

指導教授：吳文榕 博士　　Advisor：Dr. Wen-Rong Wu

中華民國九十六年七月

DISH 1015

IEEE 802.16 OFDMA 低複雜度內接收機設計

Low-Complexity Inner Receiver Design for IEEE 802.16 OFDMA Systems

研 究 生：丁偉家　　Student：Wei-Chia Ting

指導教授：吳文榕 博士　　Advisor：Dr. Wen-Rong Wu

國 立 交 通 大 學

電信工程學系碩士班

碩 士 論 文

A Thesis

Submitted to Department of Communication Engineering

College of Electrical and Computer Engineering

National Chiao-Tung University

in Partial Fulfillment of the Requirements

for the Degree of

Master of Science

In

Communication Engineering

July 2007

Hsinchu, Taiwan, Republic of China

中華民國九十六年七月

IEEE 802.16 OFDMA 低複雜度內接收機設計

Low-Complexity Inner Receiver Design for IEEE 802.16e OFDMA Systems

研究生：丁偉家　　指導教授：吳文榕 教授

國立交通大學電信工程學系碩士班

中文摘要

在 IEEE 802.16e 的接收機中，前置符元搜尋（Preamble Search）對於同步是一項需要高計算複雜度的主要運算，我們提出了一個新的演算法來達到這個目標，此法在頻域上處理訊號並可避免通道響應與雜訊的干擾，並且能達到極低的計算複雜度，此法可併以解決整數載波頻率偏移（CFO）與其他相關的同步問題。除此法之外，我們還建立上下鏈的傳接機系統包括了時空碼（STC）的實現。數據分析與模擬結果證實此法效率及同步效能皆令人滿意。

Low-Complexity Inner Receiver Design for IEEE 802.16e OFDMA Systems

Student: Wei-Chia Ting Advisor: Dr. Wen-Rong Wu

Department of Communication Engineering

National Chiao-Tung University

Abstract

In the 802.16e OFDMA receiver, a main operation in synchronization requiring high computational complexity is the preamble search. In this thesis, we propose a new algorithm to solve the problem. Our method, processing the signal in the frequency domain, is not affected by the channel response, and the computational complexity is low. Along with the method, we further propose an integer carrier frequency offset (CFO) estimation method, and other related synchronization modules. Despite the proposed new algorithms, we also build transceivers for both uplink and downlink, including space-time coding (STC). Numerical analysis and simulation results verify that the proposed algorithm is efficient and the performance of the synchronization is satisfactory.

Acknowledgment

首先誠摯的感謝指導教授吳文榕博士，老師悉心的教導使我得以一窺電信領域的深奧，不時的討論並指點我正確的方向，使我在這些年中獲益匪淺。老師對學問的嚴謹更是我輩學習的典範。

兩年裡的日子，實驗室裡共同的生活點滴，學術上的討論、言不及義的閒扯、等…感謝眾位學長姐、同學、學弟妹的共同砥礪，你/妳們的陪伴讓兩年的研究生活變得絢麗多彩。

感謝許兆元學長以及陳紹基教授實驗室的陳致良學長不厭其煩的指出我研究中的缺失，且總能在我迷惘時為我解惑，也感謝吳俊穎、高祥倫、林育丞、邱麟凱、鄒鎧駿、黃千致同學的幫忙，恭喜我們順利走過這兩年。

最後，謹以此文獻給我摯愛的雙親。

Catalog

中文摘要 ..... **I**

Abstract ..... **II**

Acknowledgment ..... **III**

Catalog ..... **IV**

Figure List ..... **VII**

Table List ..... **IX**

Abbreviations and Acronyms ..... **X**

Chapter 1: Introduction **1**

Chapter 2: Overview of IEEE 802.16 OFDMA Physical Layer **4**

2.1 SYSTEM STRUCTURE 4

2.1.1 OFDMA Symbol Description *4*

2.1.2 System Parameters *6*

2.1.3 Frame structure *7*

Time Division Duplexing (TDD) Mode 7

2.1.4 OFDMA basic terms definition *8*

2.1.5 Baseband system *11*

2.2 CHANNEL CODING 12

2.2.1 Concatenation *12*

2.2.2 Randomization *12*

2.2.3 Forward Error Correction (FEC) Coding *13*

2.2.4 Bit-interleaving *14*

2.2.5 Repetition *14*

2.2.6 Modulation *15*

2.3 SUBCARRIER ALLOCATION 15

2.3.1 DL PUSC *16*

2.3.2 UL PUSC *18*

2.3.3 Data Mapping *19*

2.3.4 DL Subcarrier Allocation *20*

2.3.5 UL Subcarrier Allocation *22*

2.3.6 Pilot and Subcarrier Randomization *23*

2.4 SMART ANTENNA TECHNOLOGIES 25

2.5 SUMMARY 26

Chapter 3: Proposed Inner Receiver Design 28

3.1 PREAMBLE STRUCTURE 28

3.2 CHANNEL MODEL 30

3.2.1 Multipath Fading Channel *30*

Main Path Delay 31

Fading 32

3.2.2 Noise *33*

3.2.3 Inter cell interference *33*

3.2.4 Frequency Offset *35*

CFO 35

SFO 36

3.3 PROPOSED INNER RECEIVER DESIGN 38

3.3.1 Packet Detection *39*

3.3.2 Frequency Synchronization *41*

3.3.3 Preamble Series Search *43*

3.3.3.1 Conventional Preamble Search Method 44

3.3.3.2 Proposed Preamble Search Method 46

3.3.4 ICFO Compensation *51*

3.3.5 Symbol Timing Offset Estimation *53*

3.3.6 Channel Estimation *53*

Chapter 4: Simulation Results **55**

4.1 PREAMBLE SEARCH 55

4.2 CARRIER FREQUENCY OFFSET 57

4.3 SFO 59

4.4 UPLINK 60

4.5 DOWNLINK USING STC 63

Chapter 5: Conclusions **64**

Reference **65**

Figure List

Figure 2-1 : OFDMA symbol time domain structure 5

Figure 2-2 : OFDMA frequency description 6

Figure 2-3: WiMAX OFDMA TDD frame structure (Figure 7 from [3]) 8

Figure 2-4 : OFDMA PUSC unit structure 10

Figure 2-5 : Baseband communication system 11

Figure 2-6 : Channel coding process 12

Figure 2-7 : PRBS for data randomization 13

Figure 2-8 : Illustration of OFDMA frame with multiple zones 16

Figure 2-9: Cluster structure 17

Figure 2-10: Description of an uplink tile 18

Figure 2-11 : Mapping subcarriers to a slot 19

Figure 2-12: Mapping slots to a burst in downlink 20

Figure 2-13 : Mapping slots to an uplink zone in uplink 20

Figure 2-14 : PRBS generator for pilot modulation and subcarrier randomization 23

Figure 2-15: Cluster structure for STC PUSC using 2 Antennas 26

Figure 2-16 : Baseband transmitter 27

Figure 2-17: Baseband receiver 27

Figure 3-1: Preamble structure in the frequency domain 29

Figure 3-2: Sine function in 3 identical parts (the number of samples is not divisible by 3) .. 30

Figure 3-3 : ISI caused by timing offset 32

Figure 3-4: Illustration of the distance between BS and cell boundaries 34

Figure 3-5: Illustration of the cell boundaries 34

Figure 3-6: Transmit and receive sampling periods 37

Figure 3-7 : SFO in cosine function 37

Figure 3-8 : SFO effect in the frequency domain 38

Figure 3-9: Delay, correlated and normalized detection algorithm 40

Figure 3-10: Response of the packet detection 41

Figure 3-11: Correlation result in time domain 45

Figure 3-12: Structure of conventional preamble search algorithm 46

Figure 3-13: Differentiation of matched result (code-matched case) 47

Figure 3-14: Differentiation of matched result (code-unmatched case) 47

Figure 3-15: Hardware implementation of proposed approach 50

Figure 4-1: False preamble detection probability of preamble search; quasi-stationary SCM channel, 2048 subcarriers, mobile speed 100~200 km/h 56

Figure 4-2: False preamble detection probability of preamble search; non-stationary SCM channel, 2048 subcarriers, mobile speed 100 km/h 57

Figure 4-3: Mean square error performance of proposed CFO estimator in an AWGN channel; 2048 subcarriers, CFO ±15 ppm 58

Figure 4-4: Mean Square Error Comparison of the proposed CFO method and the DS-WOS approach [8] in the presence of integer CFO; SCM channel, 2048 subcarriers, 1 subcarrier spacing ICFO 59

Figure 4-5: Comparison between SFO-less and SFO-compensated system (OFDMA DL) ... 60

Figure 4-6: BER performance of UL in multipath fading channel (two mobile speeds) 61

Figure 4-7: BER performance comparison for UL known channel and estimated channel 62

Figure 4-8: BER performance comparison of DL and UL (known channel) 62

Figure 4-9 : Comparison of SISO DL and STC DL (known channel) 63

Table List

Table 2-1: Mobile WiMAX system parameters 6

Table 2-2: Slot definition 9

Table 2-3 : Puncture configuration 14

Table 2-4 : 2048-FFT OFDMA downlink subcarrier allocations for PUSC 17

Table 2-5: 2048-FFT OFDMA uplink subcarrier allocations for PUSC 18

Table 3-1: Computational Complexity Comparison of conventional approach and proposed approach 51

Abbreviations and Acronyms

3GPP	3rd Generation Partnership Project
AAS	adaptive antenna system
ADC	analog to digital converter
AMC	adaptive modulation and coding
BER	bit error rate
BS	base station
BW	bandwidth
BWA	broadband wireless access
CFO	carrier frequency offset
CP	cyclic prefix
DAC	digital to analog converter
DC	direct current
DCND	delay, correlated and normalized detection
DFT	discrete Fourier transform
DL-MAP	downlink map
DS-WS	direct-search with segmentation
DS-WOS	direct-search without segmentation
FCH	frame control header
FDD	frequency division duplex
FEC	forward error correction
FFT	fast Fourier transform
FHDC	frequency hopped diversity coding
FUSC	fully usage of subchannels
IDcell	identification of cells

IDFT	inverse discrete Fourier transform
IFFT	inverse fast Fourier transform
LOS	line-of-sight
LSB	least significant bit
MAC	medium access control layer
MANs	metropolitan area networks
MSB	most significant bit
MSE	mean square error
NLOS	non-line-of-sight
OFDM	orthogonal frequency division multiplexing
OFDMA	orthogonal frequency division multiplex access
PHY	physical
PN	pseudo-noise
PRBS	pseudo-random binary sequence
PUSC	partial usage of subchannels
RF	radio frequency
SC	single carrier
SCa	single carrier access
SCM	spatial channel model
SOFDMA	scalable orthogonal frequency division multiplex access
SFO	sampling frequency offset
SM	spatial multiplexing
SNR	signal-to-noise ratio
SS	subscriber station
STC	space time coding

TDD	time division duplex
TUSC	tile usage of subchannels
UL-MAP	uplink map
WiMAX	Worldwide Interoperability for Microwave Access

Chapter 1: Introduction

Due to the growing demand of high-speed wireless data service, the IEEE 802.16 Working Group on Broadband Wireless Access (BWA) has been developing related standards and amendments, targeting for broadband Wireless Metropolitan Area Networks (MANs) since 1999.

The first revision of IEEE 802.16 standard, published in 2002, defines the air interface in medium access control (MAC) layer and physical (PHY) layer. It provides fixed point-to-multipoint broadband wireless access networks, which supports single carrier (SC) transmission in the 10-66 GHz range with only line-of-sight (LOS) capability. The following two amendments, IEEE 802.16a and IEEE 802.16c, add the support for non-LOS (NLOS) scenarios in 2-11 GHz band. The physical (PHY) standard extended the implementation of Orthogonal Frequency Division Multiplexing (OFDM) and Orthogonal Frequency Division Multiple Access (OFDMA). More system profiles for the 10-66 GHz band were also added. In 2004, a major consolidation of above three standards has been published, named the IEEE 802.16-2004 Air Interface Standard [1]. In December, 2005 IEEE ratified the 802.16e amendment [2] to the 802.16 standard. This amendment adds the features and attributes to the standard, necessary to support mobility. Scalable OFDMA (S-OFDMA) is also introduced in the IEEE 802.16e to support scalable channel bandwidths.

Similar to the role of Wi-Fi for IEEE 802.11, the WiMAX (Worldwide Interoperability for Microwave Access) Forum was formed in June 2001 for IEEE 802.16. The objective of WiMAX Forum is to facilitate the deployment of broadband wireless networks based on the IEEE 802.16 standard by ensuring the compatibility and interoperability of broadband wireless equipment. Fixed WiMAX, based on the IEEE 802.16-2004 has been proven to be a cost-effective fixed wireless alternative to wireline broadband access such as cable and DSL.

The WiMAX Forum is now defining system performance and certification profiles [3][4][5] based on the IEEE 802.16e Mobile Amendment for Mobile WiMAX, which enables the convergence of mobile and fixed broadband networks through a common wide area broadband radio access technology and a flexible network architecture.

The Mobile WiMAX Air Interface comprises 2 levels: medium access control (MAC) layer and physical (PHY) layer. The PHY layer adopts OFDMA for improving multi-path performance in NLOS environments. OFDMA shares most features of OFDM as a multiple access extension scheme. OFDM is considered as an efficient communication technique evolved from frequency-division multiplexing (FDM); it can be seen as one multi-carrier system. Today, OFDM is widely used in many communication systems such as ADSL, DVB, UWB, and WLAN. However, there are new challenges for OFDMA systems in spite of the frequency synchronization issues inherited from OFDM. The user of an OFDMA system must perform a preamble search from different Base Stations (BS) in the initial synchronization phase. The cell structure is also concerned on the cell boundaries when handover can be activated. Some approaches have been reported [6], [7], [8], in the literature; however, a faster and low-complexity solution has yet to be found.

In this thesis, we focus on the baseband synchronization design for the OFDMA mode in IEEE 802.16 specification. At the same time, we have built the transceiver for both uplink and downlink, including space time coding (STC), one of the key feature in 802.16. We propose a fast and low-complexity algorithm for the preamble search, and design other related inner receiver blocks. Finally, computer simulations are conducted to show the effectiveness of the proposed algorithms.

The rest of the thesis is organized as follows. In Chapter 2, we overview the specification of IEEE 802.16e OFDMA PHY layer, and the system profiles defined by Mobile WiMAX. In the first part of Chapter 3 discusses the possible synchronization structures of an OFDMA

system. The second part elaborates the proposed inner receiver design. In Chapter 4, simulation results are shown and analyzed. Finally, Chapter 5 gives conclusions and possible future works.

Chapter 2: Overview of IEEE 802.16 OFDMA Physical Layer

This chapter gives an overview of IEEE 802.16e OFDMA PHY layer. The purpose of the PHY is the physical transport of data between both sides in uplink and downlink. It is responsible for the transmission of the bit sequence. It defines the type of signal used, the kind of modulation and coding, the transmission power and also other physical characteristics. After processing, PHY converts the bit stream into a physical signal transmitted over a transmission medium.

2.1 System Structure

WirelessMAN-OFDMA is one of the five PHY interfaces defined in IEEE Std 802.16. It operates in the licensed frequency bands below 11 GHz, which is often considered as a NLOS scenario. In this section, we will outline the IEEE 802.16 OFDMA PHY system structure. OFDMA is the multiple access extension of OFDM, inheriting most of OFDM's characteristics.

2.1.1 OFDMA Symbol Description

(A) Time domain symbol

In spectrum below 11 GHz, a robust BWA system must deal with multipath without resorting to highly directional antennas. By copy the redundant samples from the tail, the transmitted symbol remains continuous in phase after IFFT. The IFFT can also effectively transform a set of orthogonal narrowband transmissions into a single waveform. Figure 2-1 illustrates the OFDMA symbol time domain structure.

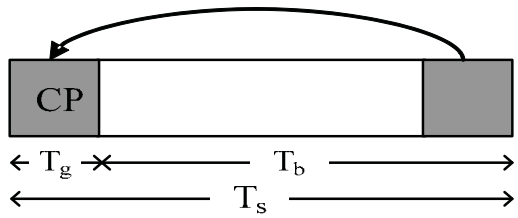

Figure 2-1 : OFDMA symbol time domain structure

The time duration is referred to as the useful symbol time T_b. A copy of the last T_g of the useful symbol period, termed CP, is added in front of the original symbol. It is used to resist multipath effect, while maintaining the orthogonality of the original symbol.

(B) Frequency domain symbol

When the subcarrier spacing is sufficiently small, the channel characteristics can be safely assumed to be constant across the subcarrier. This assumption drastically simplifies channel estimation since only one tap is required for each subcarrier.

An OFDMA symbol is made up of subcarriers, and the number of which determines the FFT size; sizes of 2048, 1024, 512, and 128 are supported. We consider only the FFT size of 2048 in this thesis. In the remainder of this thesis, the 2048-FFT will be assumed. Several subcarrier types are defined as

- Data subcarriers: for data transmission
- Pilot subcarriers: for various synchronization/estimation purposes
- Null subcarriers: no transmission, for guard bands and DC carrier

The purpose of the guard bands is to enable the signal to naturally decay and create the FFT “brick wall” shaping. Unlike OFDM, the active OFDMA subcarriers are divided into the subsets of the subcarriers; each subset is termed a subchannel. In the downlink, a subchannel may be intended for different receivers; in the uplink, a transmitter may be assigned to one or more subchannels. Subcarriers in one subchannel may not be adjacent. The concept of subchannelization is shown in Figure 2-2.

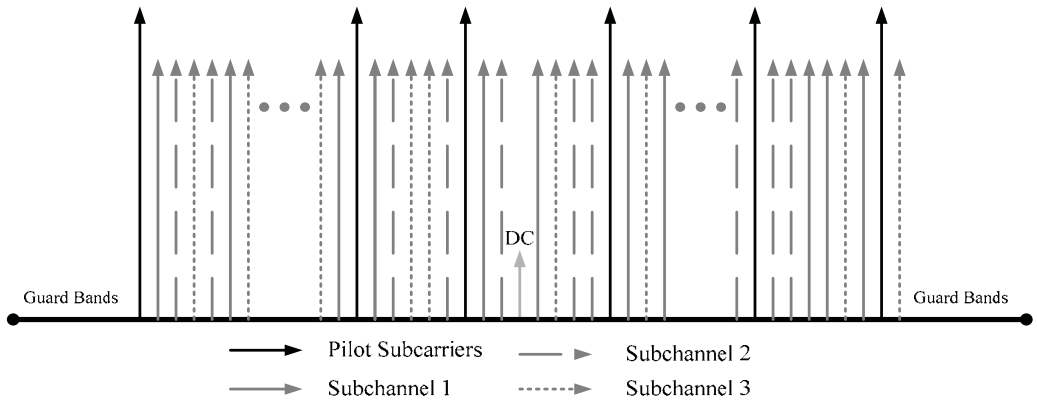

Figure 2-2 : OFDMA frequency description

2.1.2 System Parameters

The parameters of the transmitted OFDMA signal are given in Table 2.1. The first three parameters shown below are the primitive parameters characterizing the OFDM symbol. The rest of the parameters are defined in terms of the primitive parameters.

- BW: Nominal system channel bandwidth.
- N_{used}: Number of used subcarriers, including DC subcarrier.
- n: Sampling factor. This parameter, in conjunction with BW, determines the subcarrier spacing, and the useful symbol time. This value is generally set to 28/25 in Mobile WiMAX [3].

Table 2-1: Mobile WiMAX system parameters

Parameters	Values					
N_{FFT}	128	512	1024	2048	1024	
BW (MHz)	1.25	5	10	20	7	8.75
n	28/25				8/7	8/7
F_s (MHz)	1.4	5.6	11.2	22.4	8	10
Number of Subchannels	2	8	16	32	16	16
Subcarrier Spacing (kHz)	10.94				7.81	9.77
Useful Symbol Time T_b	91.4 microseconds				128.04	102.4
Guard Time T_g (G = 1/8)	11.4 microseconds				16.00	12.8
OFDMA Symbol Duration T_s	102.9 microseconds				144.05	115.2

Number of OFDMA Symbols (5 ms Frame)	48	34	43

- G: This is the ratio of CP time to "useful" time. The following values are supported: 1/32, 1/16, 1/8 and 1/4. 1/8 is used in [3].
- N_{FFT}: FFT size of the OFDM symbol.
- Sampling Frequency: $F_S = floor(n \cdot BW / 8000) \times 8000$
- Useful symbol time: $\Delta f = F_S / N_{FFT}$
- CP time: $T_b = 1/\Delta f$
- OFDMA symbol time: $T_S = T_b + T_g$
- Sampling time: T_b / N_{FFT}

Scalable OFDMA

OFDMA PHY is said to have Scalable OFDMA (S-OFDMA). The scalability is the change of the FFT size and the number of subcarriers. The change in the number of subcarriers provides for an adaptive transmission bandwidth and an adaptive data rate. S-OFDMA provides additional resource allocation flexibility according to the dynamic spectrum demand as a radio resource management.

2.1.3 Frame structure

Time Division Duplexing (TDD) Mode

The WiMAX/802.16 standard includes the two main duplexing techniques: TDD and FDD. The choice of duplexing technique may affect certain PHY parameters and influence the supported features. TDD is the only duplexing mode defined in the initial release of Mobile WiMAX certification profiles [5]. In Mobile WiMAX system profiles, only 5ms duration is mandatory. We will only consider the TDD mode in this thesis.

In the case of TDD, UL and DL transmissions share the same frequency but they take place at different times. Figure 2-3 illustrates the OFDMA TDD frame structure. Each frame

is divided into DL and UL sub-frames, separated by Transmit/Receive and Receive/Transmit Transition Gaps (TTG and RTG, respectively), preventing DL and UL transmission collisions. In a frame, the following control information is used to ensure optimal system operation:

- Preamble: The preamble, used for synchronization, is the first OFDM symbol of the frame. We will discuss more details about preamble in Chapter 3.

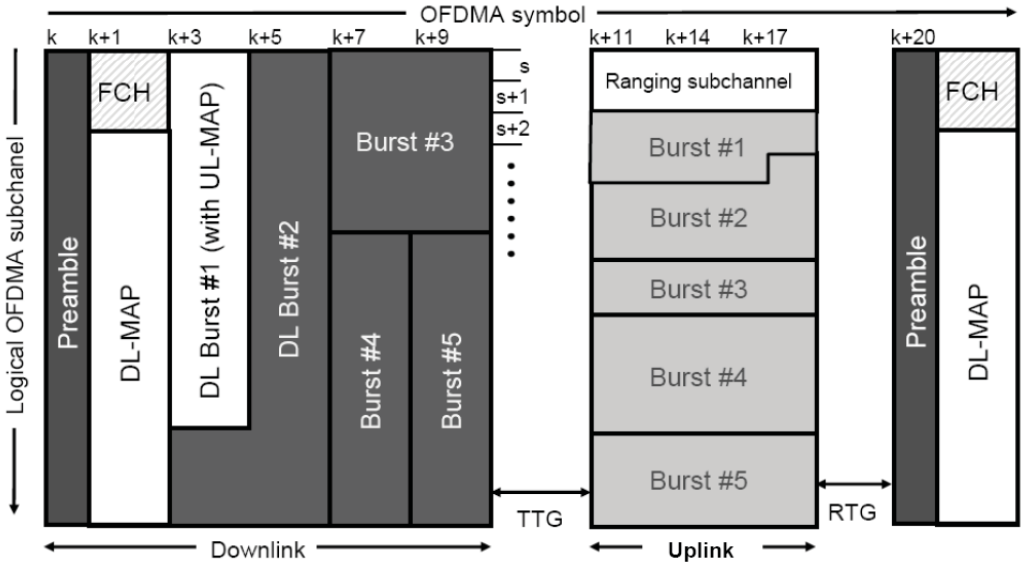

Figure 2-3: WiMAX OFDMA TDD frame structure (Figure 7 from [3])

- Frame Control Header (FCH): The FCH follows the preamble. It provides the frame configuration information such as MAP message length and coding scheme, and usable sub-channels. It is transmitted as QPSK symbols using the mandatory coding scheme with rate 1/2 and four repetitions.
- DL-MAP and UL-MAP: They provide sub-channel allocation and other control information for the DL and UL sub-frames respectively.
- UL Ranging: The UL ranging sub-channel is allocated for mobile stations (MS) to perform closed-loop time, frequency, and power adjustment as well as bandwidth requests.

2.1.4 OFDMA basic terms definition

There are various processing units in OFDMA since the MAC data are mapped

two-dimensionally on time and frequency domains. We briefly describe basic OFDMA terms in this subsection.

One-dimension units:

- OFDMA signal: The most basic unit on time domain, as defined in 2.1.1
- Subcarrier (Tone): The most basic unit on frequency domain, as defined in 2.1.1
- Subchannel: In OFDMA, subcarriers are divided into subsets of subcarriers, each subset representing a subchannel as shown in Figure 2-2. Each of the permutation modes of OFDMA has its definition for a subchannel.

Two-dimension units:

- Slot: The minimum possible data allocation unit in the time-frequency domain. A slot always consists of a single subchannel, but, depending on the physical mapping, consists of one to three OFDMA symbols. See Table 2-2 for its definitions.

Table 2-2: Slot definition

Permutation mode	Slot definition
DL FUSC; DL OFUSC	1 subchannel × 1 OFDMA symbol
DL PUSC	1 subchannel × 2 OFDMA symbol
DL TUSC1,DL TUSC2 UL PUSC, UL OPUSC	1 subchannel × 3 OFDMA symbol
AMC (both DL and UL)	1 subchannel × 1 OFDMA symbol

- Cluster/Tile/Bin: A special time-frequency unit used for specific subcarrier allocation scheme. Cluster is the unit for DL PUSC; while Tile is the unit for UL PUSC. Bin is used for AMC.
- Burst (Data Region): It is a two-dimensional allocation of a group of slots in the time-frequency domain. Every burst has its own modulation and coding scheme.
- Segment: A segment is a subdivision of the set of available subchannels, controlled by a

single instance of the BS MAC. Due to the use of sectorization antennas, there are three segments. Every segment has its own subchannel groups.

- Permutation Zone: It is a number of contiguous OFDMA symbols that use the same permutation mode. A downlink subframe or an uplink subframe may contain more than one permutation zones.

- Frame: Frame is a structure data sequence and contains both the uplink subframe and the downlink subframe.

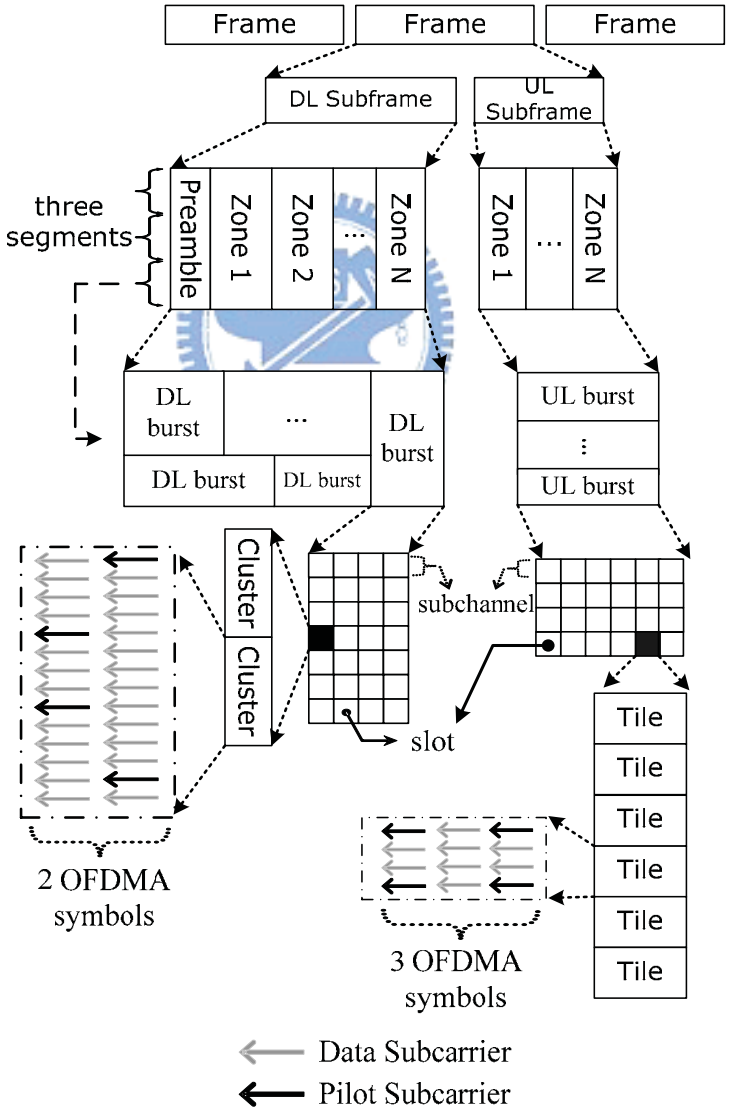

Figure 2-4 : OFDMA PUSC unit structure

2.1.5 Baseband system

The baseband system represents the whole physical layer except for the analog and RF sections. For both downlink and uplink transmitters, the baseband system can be roughly divided into two or three modules:

- Channel coding
- Subcarriers allocation
- Transmit diversity coding (optional)

In the receiver, it is mainly divided two modules: inner receiver and outer receiver. The outer receiver is further divided into modules as that in the transmitter. In OFDMA, inner receiver performs preamble search, timing synchronization, and frequency synchronization. Figure 2-5 illustrates the architecture of the baseband processing system. Due to the lack of preamble in uplink, the inner receiver in the base station is simpler to design. The uplink synchronization will be conducted during the contention.

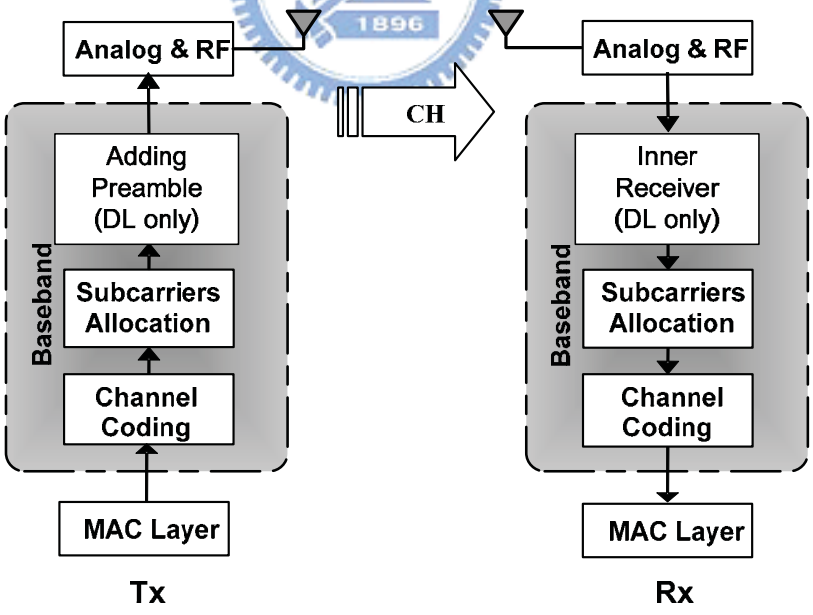

Figure 2-5 : Baseband communication system

Operations of the transmitter and the outer receiver will be discussed in this chapter. The operation of the inner receiver will be explained in Chapter 3.

2.2 Channel Coding

The radio link is a rapidly varying link, often suffering from great interference. The main tasks of channel coding are to prevent and to correct the transmission errors generated by radio link interferences. The 802.16 OFDMA channel encoding consists of randomization, FEC, interleaving, repetition, and modulation. These operations are shown in Figure 2-6. The corresponding operations at the receiver are applied in the reverse order. In this section, we only make a brief description of each block. Further information can be obtained through [1], [2] and [7].

Figure 2-6 : Channel coding process

2.2.1 Concatenation

Concatenation is a function of concatenating multiple MAC PDUs into a single PHY burst in order to reduce the overhead. It divides one data burst into blocks. If the content of MAC PDU does not fit exactly the size of allocated burst, a padding of 0xFF ("all 1") must be conducted to the end of the block to fill the blank. Concatenation is possible in both UL and DL.

2.2.2 Randomization

Randomization is a function that randomizes the data to avoid non-centered data sequences which are composed of consecutive ones or zeros. Such sequences result in a high PAPR for the OFDM symbol. Randomization is performed by passing the block of data to be transmitted through a pseudo-random binary sequence (PRBS) with polynomial $1+x^{14}+x^{15}$, as shown in Figure 2-7. For each FEC block, the same fixed initialization value is used, regardless of when and where it is transmitted. However, the objective to reduce PAPR is can

also be achieved in the OFDMA PHY due to the logical to physical permutations and the different time-frequency allocation that may be used when retransmitting the data.

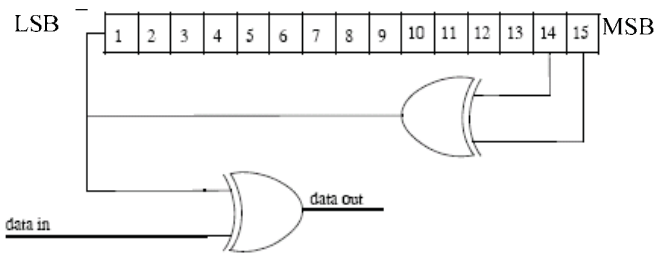

Figure 2-7 : PRBS for data randomization

The randomizer is initialized with the vector: [LSB] 0 1 1 0 1 1 1 0 0 0 1 0 1 0 1 [MSB]. Data randomization is performed on all data transmitted, downlink and uplink, except for those in the FCH.

2.2.3 Forward Error Correction (FEC) Coding

For OFDMA PHY, the FEC encodings are:

- (Tail-biting) Convolutional Code (CC): This code is mandatory in 802.16 standard. According to WiMAX profiles, only the Zero-Tailing Convolutional Code (ZT CC) is mandatory.
- Convolutional Turbo Codes (CTC): This code is optional in 802.16 standard but mandatory in mobile WiMAX profiles
- Block Turbo Coding (BTC): This code is optional.
- Low Density Parity Check (LDPC) codes: This code is optional.

In tail-biting CC, the convolutional encoder memories are initialized by the last six data bits of the FEC block being encoded. It avoids the 1 byte of tail overhead employed by optional zero tailing CC in the cost of increased computation for decoder.

After randomization, each FEC block is encoded by the binary convolutional encoder, which have native rate of 1/2, a constraint length equal to K=7. The following generator polynomials are used to derive its two coded bits:

$$G_1 = 171_{OCT} \quad \text{For } X$$
$$G_1 = 133_{OCT} \quad \text{For } Y$$

The puncturing patterns and serialization order that is used to realize different code rates defined in Table 2-3. In the figure, "1" means a transmitted bit and "0" denotes a removed bit.

Table 2-3 : Puncture configuration

Code Rates	1/2	2/3	3/4
$\mathbf{d_{free}}$	10	6	5
X	1	10	101
Y	1	11	110
XY	X_1Y_1	$X_1Y_1Y_2$	$X_1Y_1Y_2X_3$

2.2.4 Bit-interleaving

Interleaving is used to protect the transmission against long sequences of consecutive errors, which are very difficult to correct. These long sequences of error may affect many bits in a row and result in lots of transmitted burst losses. By including some diversity, interleaving can facilitate error correction. The interleaver is made of two steps:

1. Ensures that adjacent coded bits are mapped onto nonadjacent subcarriers.

2. Ensures that adjacent coded bits are mapped alternately onto the least or most significant bits of the constellation, thus avoiding long runs of low reliability bits.

2.2.5 Repetition

Repetition can be used to increase signal margin over the original modulation and FEC mechanisms. Let the repetition factor be R, which can be 2, 4, or 6. For the uplink, the allocated slots are repeated R times.

Thus, the binary data that fit into a region that is repetition coded is reduced by a factor R compared to an unrepeated region of the slots with the same size and FEC code type. After FEC and bit-interleaving, the data is partitioned into slots, and each group of bits designated to fit in a slot will be repeated R times to form R contiguous slots following the normal slot ordering that is used for data mapping. The repetition scheme applies only to QPSK modulation and all coding schemes except HARQ with CTC.

2.2.6 Modulation

Four modulations are supported by the IEEE 802.16 standard: BPSK, QPSK, 16-QAM and 64-QAM. It is simple to see that the larger the constellation size, the more spectrum efficient but less robustness to interference we will have. With different constellation sizes, link adaptation can then be used. If the radio link is in good condition, we can then use a modulation with larger constellation size, and vice versa.

- BPSK: One bit/modulation symbols. It gives high immunity against noise and interference as a very robust modulation. BPSK is only used for preambles and ranging signals in OFDMA.
- QPSK: 2 bits/modulation symbols. QPSK is less noise resistant than BPSK as it has a smaller immunity against interference, but higher spectral efficiency.
- 16-QAM: 4 bits/modulation symbol.
- 64-QAM: 6 bits/modulation symbol. 64-QAM is optional for OFDMA PHY, yet the Mobile WiMAX profiles subsume 64-QAM as mandatory.

2.3 Subcarrier Allocation

In the OFDMA PHY, the mapping of data to physical subcarriers occurs in two steps. In the first step, dictated by the scheduler, data are mapped to one or more data slots on one or

more logical subchannels. We call this step “Data Mapping”. In the second step, for each data slot, each logical subchannel is then mapped to a number of physical subcarriers, with a mapping that may vary from one OFDM symbol to the next. The second step is termed as “subcarrier allocation” or “permutation”.

Subcarrier allocation can be categorized in the following modes: partial usage of subchannels (PUSC) and full usage of the subchannels (FUSC) in the downlink, PUSC in the uplink, and other optional usages. PUSC is corresponds to allocate some of the subchannels to the transmitter; FUSC to allocate all subchannels to the transmitter. As shown in Figure 2-8, a single frame may contain one or more permutation zones. The first DL zone must be the PUSC zone because the MS does not have any message regarding allocation before first zone. The first PUSC zone must be QPSK modulated 1/2 CC coded with repetition 4. This thesis focuses on the subcarrier allocation of DL-PUSC and UL-PUSC.

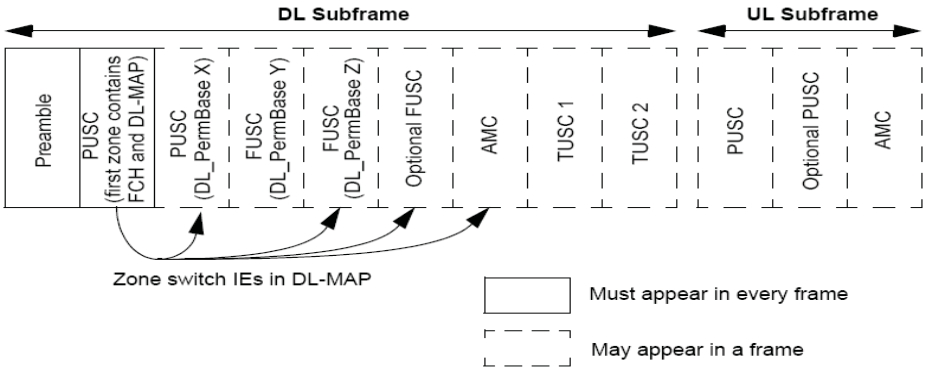

Figure 2-8 : Illustration of OFDMA frame with multiple zones

2.3.1 DL PUSC

For DL PUSC, the pilot tones are allocated first. What remains are data subcarriers, which are divided into subchannels that are used exclusively for data. There is one set of common pilot subcarriers for each major group including a set of subchannels in DL PUSC.

Figure 2-9 depicts the cluster structure.

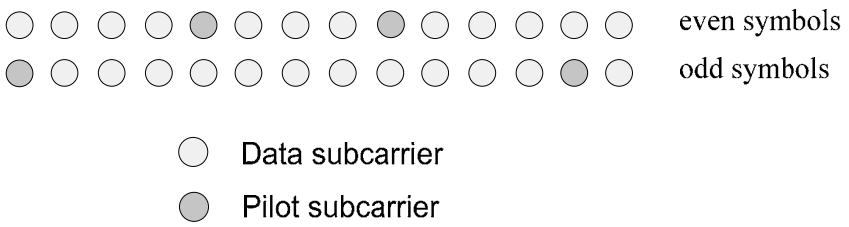

Figure 2-9: Cluster structure

Table 2-4 : 2048-FFT OFDMA downlink subcarrier allocations for PUSC

Parameter	Value	Comments
Number of DC subcarriers	1	Index 1024 (counting form 0)
Guard subcarriers: Left, Right	184,183	
Number of used subcarriers (N_{used})	1681	Number of all subcarriers used within a symbol, including all possible allocated pilots and the DC carrier.
Number of subcarriers per cluster	14	2 are pilot subcarriers.
Number of cluster	120	
Renumbering sequence	1	Used to renumber clusters before allocation to subchannels. Details can be found in [1] and [2].
Number of data subcarriers in each symbol per subchannel	24	
Number of subchannels	60	
Basic permutation sequence 12 (for 12 subchannels)		6,9,4,8,10,11,5,2,7,3,1,0
Basic permutation sequence 8 (for 12 subchannels)		7,4,0,2,1,5,3,6

Figure 2-4 shows the partition from a frame to a subcarrier in frequency domain. One frame of used subcarriers (1680 subcarriers excluding DC) is divided into three segments, each segment of 560 subcarriers is divided into 20 subchannels, each subchannel of 28 subcarriers is divided into two clusters, and each cluster (14 subcarriers) is divided into 12 data subcarriers and 2 pilot subcarriers. The location of the pilot subcarrier is also depicted in the figure. Note that the slot and the cluster are two-dimensional, and one cluster corresponds to exactly a half slot.

2.3.2 UL PUSC

For UL PUSC, the set of used subcarriers is first partitioned into subchannels and then the pilot subcarriers are allocated from with each subchannel. Each subchannel contains its own set of pilot subcarriers.

Table 2-5: 2048-FFT OFDMA uplink subcarrier allocations for PUSC

Parameter	Value	Comments
Number of DC subcarriers	1	Index 1024 (counting form 0)
Guard subcarriers: Left, Right	184,183	
Number of used subcarriers (N_{used})	1681	Number of all subcarriers used within a symbol, including all possible allocated pilots and the DC carrier.
Number of tiles (N_{tiles})	420	
Number of subchannels	70	
Number of tiles per slot	6	
Number of subcarriers per tile	12	4 are pilot subcarriers.
Number of subcarriers per slot	72	24 are pilot subcarriers
$N_{subcarriers}$	48	Number of data subcarriers per slot
TilePermutation		Used to renumber tiles. Details can be found in [1] and [2].

A slot in the uplink is composed of three OFDMA symbols and one subchannel, within each slot, there are 48 data subcarriers and 24 fixed-locations pilots. The subchannel is constructed from six uplink tiles, each tile has four successive active subcarriers and its configuration is illustrated in Figure 2-10.

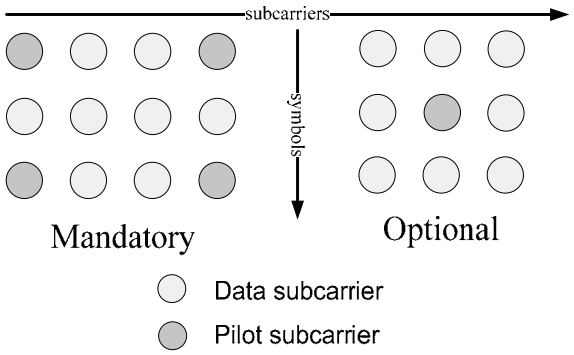

Figure 2-10: Description of an uplink tile

2.3.3 Data Mapping

After modulation, the constellation-mapped data are subsequently allocated onto slots and then to the burst area (OFDMA data region). The subcarrier allocation within a slot uses the algorithms described below, as also depicted in Figure 2-11. The slot mappings of DL and UL are depicted in Figure 2-12 and Figure 2-13, respectively.

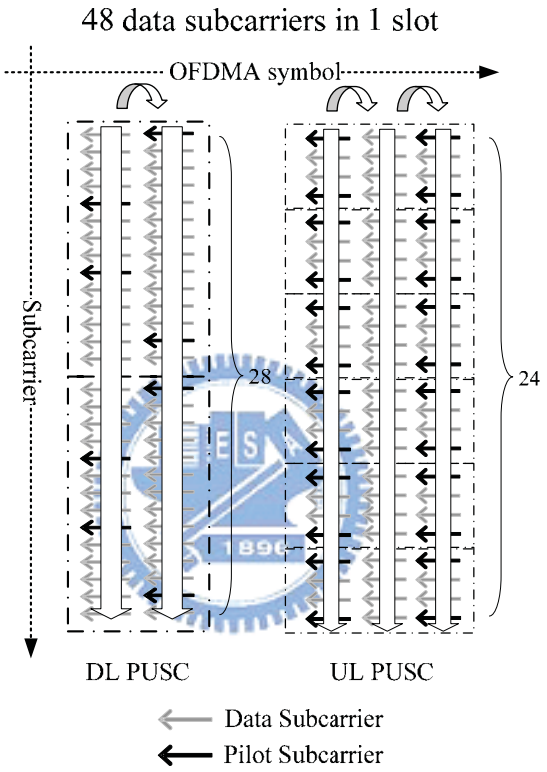

Figure 2-11 : Mapping subcarriers to a slot

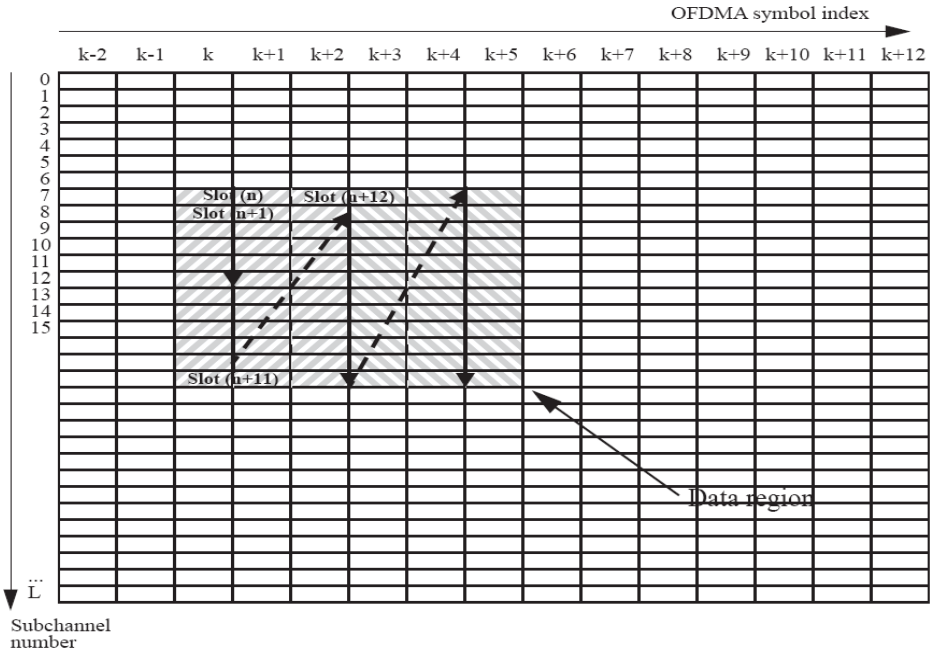

Figure 2-12: Mapping slots to a burst in downlink

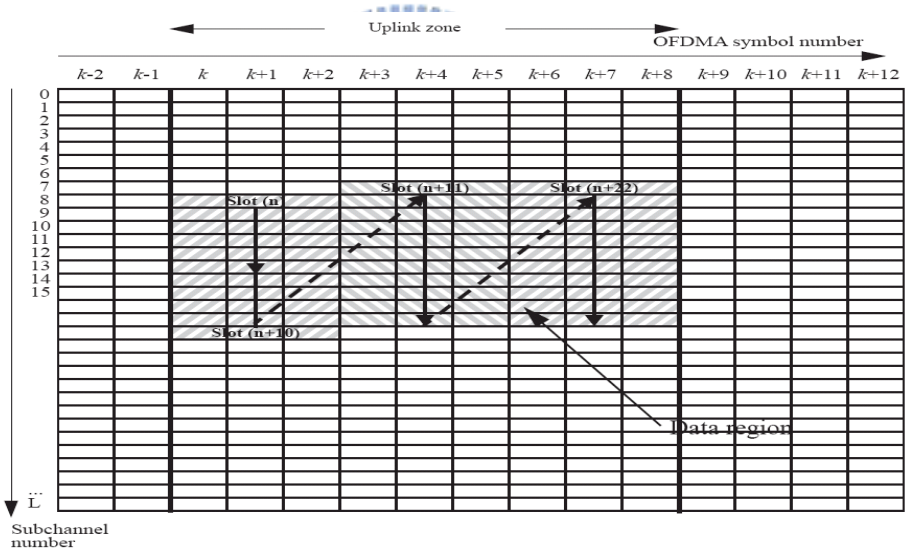

Figure 2-13 : Mapping slots to an uplink zone in uplink

2.3.4 DL Subcarrier Allocation

Permutation

The permutation is a function similar to the subcarrier interleaving. It exchanges the location of subcarriers to resist frequency-selected channel fading.

One segment is divided into one big group of 12 subchannels and another small group of

8 subchannels. The number of subchannels per group is denoted $N_{subchannels}$ and the number of subcarriers per subchannel is denoted $N_{subcarriers}$. As mentioned, one subchannel contains 24 data subcarriers in PUSC. Then, allocate subcarriers in each group to subchannels for each OFDMA symbol using (2-1), called a permutation formula.

$$\begin{aligned} &subcarrier(k,s) \\ &= N_{subchannels} \cdot n_k + \{p_s[n_k \bmod N_{subchannels}] + DL_PermBase\} \bmod N_{subchannels} \end{aligned} \tag{2-1}$$

, where

$sbucarrier(k,s)$	is the subcarrier index of subcarrier k in subchannel s,
k	is the subcarrier-in-subchannel index form the set $[0 \ldots N_{subcarriers}\text{-}1]$,
s	is the index number of a subchannel, from the set $[0 \ldots N_{subchannels}\text{-}1]$,
n_k	$= (k + 13 \cdot s) \bmod N_{subcarriers}$
$N_{subchannels}$	is the number of subchannels, 12 in even group and 8 in odd group
$N_{subcarriers}$	is the number of data subcarriers per subchannel in each OFDMA symbol,
$p_s[j]$	is the series obtained by rotating basic permutation sequence cyclically to the left s times,
DL_PermBase	is an integer ranging from 0 to 31, which is set to preamble IDcell in the first zone and determined by the DL-MAP for other zones

In initialization, an subscriber station (SS) must search for the downlink preamble. After finding the preamble, the SS will know the IDcell used for the permutation.

Renumbering

Since PUSC subcarrier permutation is conducted in each group separately, subcarriers will not be exchanged among groups. The function of the renumbering is to interleave subcarriers among groups. Renumbering uses a cluster as the basic unit to exchange the logical clusters into physical clusters using (2-2):

$$LogicalCluster = \begin{cases} \text{RenumberingSequence}(PhysicalCluster), \text{ First DL zone} \\ \text{RenumberingSequence}((PhysicalCluster + 13 \cdot DL_PermBase) \bmod 120), \text{o.w.} \end{cases} \quad (2\text{-}2)$$

2.3.5 UL Subcarrier Allocation

Permutation

The mapping of data onto the subcarriers will follow (2-3). This equation calculates the subcarrier index to which the data constellation point is to be mapped.

$$subcarrier(n,s) = (n + 13 \cdot s) \bmod N_{subcarriers} \quad (2\text{-}3)$$

, where

$subcarrier(n,s)$	is the permutated subcarrier index corresponding to data subcarrier n and subchannel s,
n	is a running index 0…47, indicating the data constellation point,
s	is a running index 0…69, indicating subchannel number,
$N_{subcarriers}$	is the number of subcarriers per slot.

Renumbering

The usable subcarriers in the allocated frequency band shall be divided into N_{tiles} physical tiles as defined in Figure 2-10 with parameters from Table 2-5. The logical tiles are mapped to physical tiles in the FFT using.

$$Tiles(p,q) = N_{subchannels} \cdot q + \left(Pt[(p+q) \bmod N_{subchannels}] + UL_PermBase\right) \bmod N_{subchannels} \quad (2\text{-}4)$$

, where

$Tile(p,q)$	is the physical tile index in the FFT with tiles being ordered consecutively from the negative to the most positive used subcarrier (0 is the starting tile index)
p	is the tile index 0…5 in a subchannel
q	is the subchannel number in the range $0,...,N_{subchannels}-1$
Pt	is the tile permutation
UL_PermBase	is an integer value in the range 0…69, which is assigned by a management entity
$N_{subchannels}$	is the number of subcarriers per slot.

2.3.6 Pilot and Subcarrier Randomization

Pilots, similar to the preamble, are known by the receiver before data transmission. They are inserted into data sequence and can be used by the receiver for synchronization and channel estimation.

The subcarrier randomization is different from the data randomization. The values of pilots and data subcarriers are generated from the same PRBS sequence. Signals in subcarriers will be multiplied by the sequence to achieve randomization effect. The PRBS generator depicted in Figure 2-14 should be used to produce a sequence, 'w_k', where 'k' is the physically (after renumbering) used subcarrier index. The polynomial for the generator is '$X^{11}+X^9+1$'.

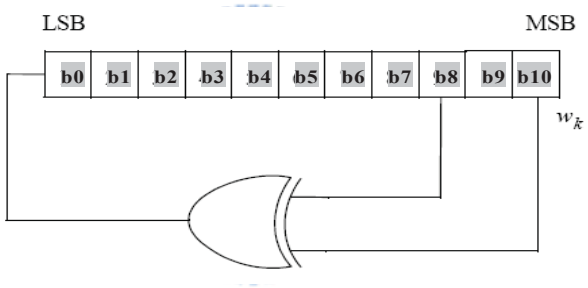

Figure 2-14 : PRBS generator for pilot modulation and subcarrier randomization

The initialization vector of the PRBS generator for both uplink and downlink is designated as b10~b0, such that:

- b0~b4 = Five least significant bits of IDcell as indicated by the frame preamble in the first downlink zone and in the downlink AAS zone with Diversity_Map support, DL_PermBase following STC_DL_Zone_IE, and 5 LSB of DL_PermBase following AAS_DL_IE without Diversity_Map support in the downlink. Five least significant bits of IDcell (as determined by the preamble) in the uplink. For downlink and uplink, b0 is MSB and b4 is LSB, respectively.
- b5~b6 = Set to the segment number + 1 as indicated by the frame preamble in the first

downlink zone and in the downlink AAS zone with Diversity_Map support, PRBS_ID as indicated by the STC_DL_Zone_IE or AAS_DL_IE without Diversity_Map support in other downlink zones, and 0b11 in the uplink. For downlink and uplink, b5 is MSB and b6 is LSB, respectively.

- b7~b0 =0b1111 (all ones) in the downlink and four least significant bits of the Frame Number in the uplink. For downlink and uplink, b7 is MSB and b10 is LSB, respectively.

For example, the initialization vector of the PRBS generator is b10~b0 = 10101010101, the result in the sequence w_k = 1010101010100000… in the uplink.

After generating w_k, the pilot subcarrier c_k should be modulated according to following equations.

- For the mandatory tile structure in the uplink:

$$\begin{aligned} \mathrm{Re}\{c_k\} &= 2\cdot\left(\frac{1}{2}-w_k\right) \\ \mathrm{Im}\{c_k\} &= 0 \end{aligned} \tag{2-5}$$

- For downlink PUSC, each pilot shall be transmitted with a power boosted of 2.5 dB higher than the average non-boosted power of each data tone:

$$\begin{aligned} \mathrm{Re}\{c_k\} &= \frac{8}{3}\cdot\left(\frac{1}{2}-w_k\right) \\ \mathrm{Im}\{c_k\} &= 0 \end{aligned} \tag{2-6}$$

The subcarrier randomization is accomplished as each modulated data subcarrier is multiplied by the factor $2\left(\frac{1}{2}-w_k\right)$. In DL PUSC, we can combine the pilot and data subcarrier randomization by inserting the value of 4/3 into pilot subcarriers and then multiplying both pilot and data subcarriers with the same factor $2\left(\frac{1}{2}-w_k\right)$.

2.4 Smart Antenna Technologies

For operations below 11 GHz, the IEEE 802.16 standard provides support for advanced multi-antenna systems, including adaptive antenna systems (AAS), and open-loop transmit diversity methods such as, space-time coding (STC), spatial multiplexing (SM), and frequency hopped diversity coding (FHDC).

We choose STC as our multiple antenna scheme. STC uses the optimal space-time block code presented by Alamouti [9], which achieves channel capacity. The STC coding gain can be used to increase spatial diversity. For simplicity, we assume that there are two transmit antennas in the BS side and one reception antenna in the SS side. Decoding of this scheme is very similar to maximum ratio combining.

STC encoding shall be performed after constellation mapping and before subcarrier randomization. s_0 and s_1 represent two subcarriers at the same frequency in two consecutive OFDMA symbols (each OFDMA subcarrier is referred to as a channel use). The STC coding is done on all data subcarriers that belong to an STC coded burst in the two OFDMA symbols. Pilot subcarriers are not encoded and are transmitted from either antenna 0 or antenna 1.

The regular subchannel and preamble transmission in the downlink shall be performed from only one antenna (Antenna 0) while the transmit diversity subchannels transmission shall be performed from both antennas obeying STC encoding formulas.

The operation of STC is described as follows: Data for two subsequent OFDMA symbols s_0 and s_1 are collected after the modulation stage, where the pilot modulations are the same for the first and second symbol. After subcarrier allocation, the first OFDMA symbol of the STC block, s_0 is transmitted from the first antenna and s_1 is transmitted from the second antenna. During the second OFDMA symbol of the STC block, the first OFDMA symbol of the STC block, $-s_1^*$ is transmitted from the first antenna and s_0^* is transmitted from the

second antenna. The channel is assumed to be constant during the two-symbol interval.

The received signals r_0 and r_1 from each antenna during two symbol periods can be denoted as

$$\begin{bmatrix} r_0 \\ r_1 \end{bmatrix} = \begin{bmatrix} s_0 & s_1 \\ -s_1^* & s_0^* \end{bmatrix} \cdot \begin{bmatrix} h_0 \\ h_1 \end{bmatrix} \tag{2-7}$$

The receiver then applies the following transform to achieve the estimates using the channel estimates $\hat{h}_0$ and $\hat{h}_1$:

$$\begin{bmatrix} \hat{s}_0 \\ \hat{s}_1 \end{bmatrix} = \begin{bmatrix} \hat{h}_0^* & \hat{h}_1 \\ \hat{h}_1^* & -\hat{h}_0 \end{bmatrix} \cdot \begin{bmatrix} r_0 \\ r_1^* \end{bmatrix} \tag{2-8}$$

For the pilots, different sequences apply to odd and even OFDMA symbols, but the pilots are placed on the same subcarriers in both symbols. This is described in Figure 2-15.

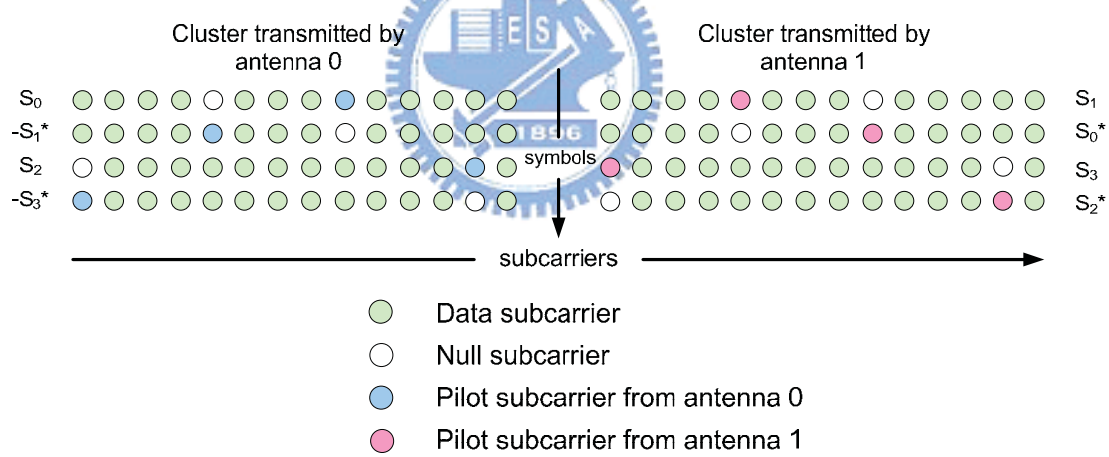

Figure 2-15: Cluster structure for STC PUSC using 2 Antennas

2.5 Summary

In this chapter, we complete the whole baseband processing for both transmitter and receiver. Figure 2-16 illustrates the OFDMA PHY transmitter architecture in PUSC.

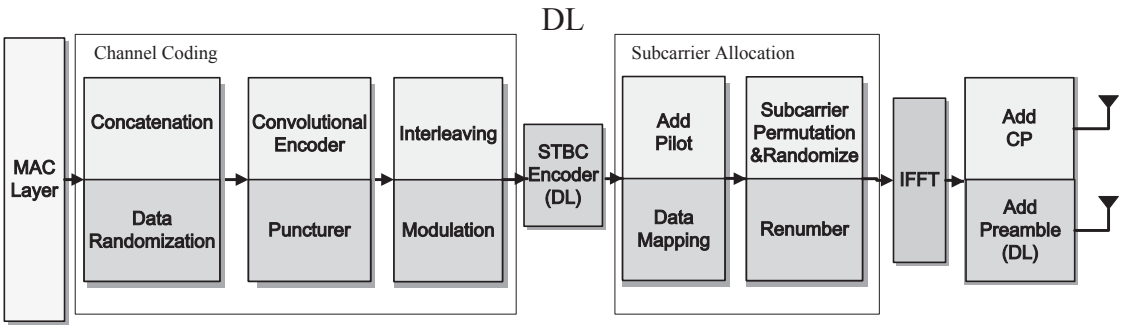

Figure 2-16 : Baseband transmitter

Figure 2-17 illustrates the OFDMA PHY receiver architecture in DL PUSC. It consists of an inner and outer receiver. The outer receiver reverses the operation conducted in the transmitter, while the inner receiver performs synchronization, channel estimation, and equalization.

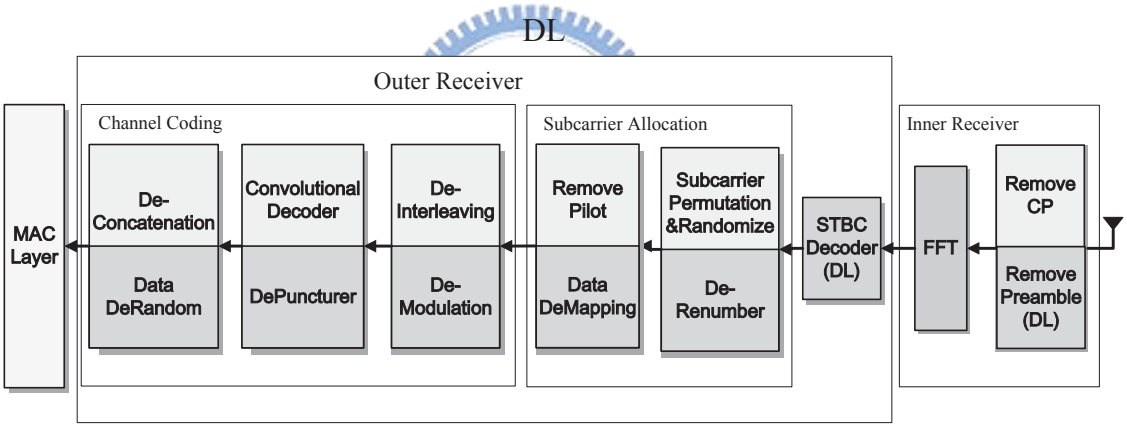

Figure 2-17: Baseband receiver

Chapter 3: Proposed Inner Receiver Design

Synchronization is of great importance to OFDM systems. Similar to OFDM, OFDMA is sensitive to carrier frequency offsets and timing errors. The OFDMA systems have to perform preamble searching due to the lack of known preamble symbol. However, the situation becomes much more complex for the MS on cell boundaries, where the SNR is typically very low.

In this Chapter, we will first describe the structure of the OFDMA downlink preamble sequences. Then, we consider channel environments on the cell boundaries and related synchronization issues. Then we propose our inner receiver design to deal with the problems. The FFT size used here is 2048, and the corresponding system profiles used are given in Chapter 2.

3.1 Preamble Structure

The first symbol of the downlink subframe is the preamble. It is used for initial synchronization and identification of the segment number. Subcarriers in the preamble are divided into three carrier-sets, each represents a different segment. The preamble carrier-sets are defined as below

$$\text{PreambleCarrierSet}_{\text{n}} = s + 3 \cdot k \tag{3-1}$$

, where

$\text{PreambleCarrierSet}_{\text{n}}$	specifies all subcarriers allocated to the specific preamble
s	in the number of the preamble carrier-set indexed 0~2
k	is a running index 0~567

The preamble subcarriers are modulated using a boosted BPSK modulation with a specific Pseudo-Noise (PN) code. These preamble modulation series are specified in Table

309, 310, 311, 312 in [1] and [2]. In each table, every segment has 38 preamble series, summing up to a total number of 114. The segment number and the ID cell are the main factors determining which preamble series to use. The series is hexadecimal and should be converted to binary before modulation on the subcarriers.

The preamble from each segment will occupy only one third of the available subcarriers. For illustration, we assume that the preamble received is for segment 0. Figure 3-1 shows the subcarrier locations the preamble signal uses. The subcarrier locations for segment 1 are one subcarrier right shifted from those of segment 0, while those for segment 2 are two subcarriers right shifted. The guard bands of the preamble vary from the FFT sizes. We can see that for 2048 size, there are 172 subcarriers on the each side of the guard band.

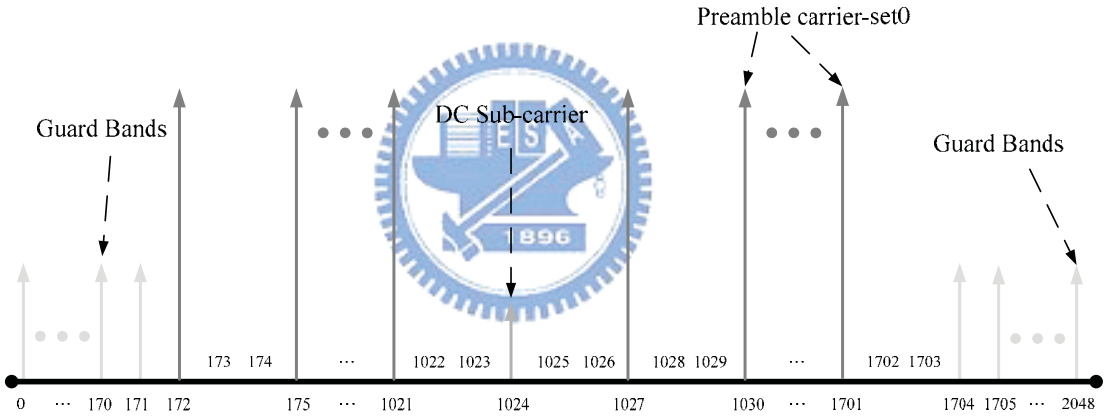

Figure 3-1: Preamble structure in the frequency domain

From the subcarrier locations, we can see that the preamble can be seen as a down-sampled signal with a factor of 3. This leads to a periodic signal in the time domain similar to the preamble used in IEEE802.11. It is simple to see that the time-domain preamble waveform has three periods. We can then exploit this property to conduct synchronization. However, the FFT size is always a power of two, which is not divisible by three. In other words, the time-domain waveform is not exactly periodic. Figure 3-2 shows a single tone signal from 0 to 6π, giving three periods. As we can see in the figure, the sampling errors do exist between the three periods.

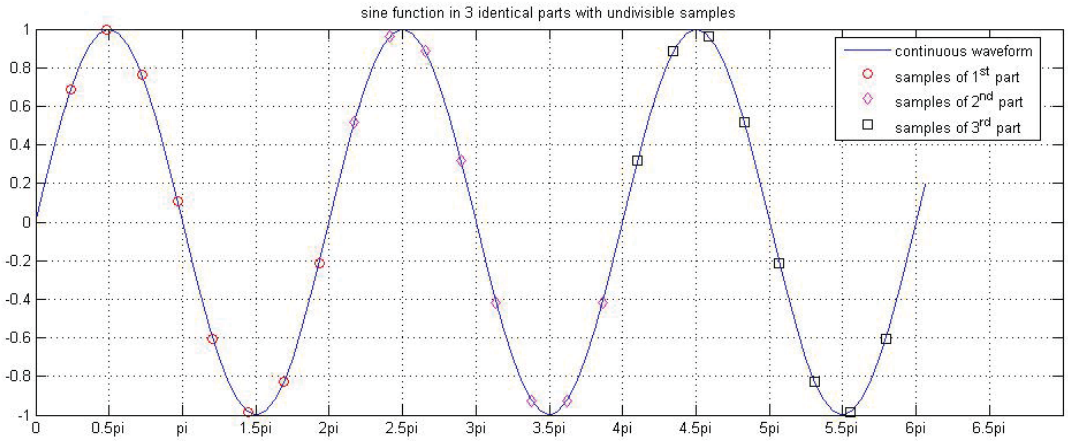

Figure 3-2: Sine function in 3 identical parts (the number of samples is not divisible by 3)

3.2 Channel Model

The physical channel effect can be divided two parts: the effect due to actual signal propagation channel, and that due to the non-ideal analog and RF components. The first one contributes to multipart channel fading and the transmission delay, while the second part to noises, carrier frequency offset, sampling offset, and nonlinear RF effects. In the receiver, we then have to use various signal process algorithms to compensate for these effects.

3.2.1 Multipath Fading Channel

OFDMA works on the frequency band under 11 GHz, in which the propagation often occurs as NLOS. As a result, the receiver may receive signal experiencing reflections or diffractions on multiple paths. These multiple-components signals arrive with different delay, amplitude, and phase, causing constructive or destructive signal combination at the receiver. In general, destructive combination is known as multipath fading.

The received signal can be modeled in the time domain as:

$$r[n] = \sum_i h_i[n] \cdot s[n - \tau_i] + w[n] \tag{3-2}$$

$$\mathbf{r} = \mathbf{h} * \mathbf{s} + \mathbf{w} \tag{3-3}$$

, where $r[n]$ denotes the received signal, $h[n]$ the channel impulse response, $s[n]$ the transmitted signal, $w[n]$ is AWGN, i the path index, τ_i the delay spread of i th multiple components, and n the sample index. In the frequency domain, the received signal can be written as:

$$R[k] = H[k] \cdot S[k] + W[k] \tag{3-4}$$

, where $R[k]$ denotes the received frequency-domain signal, $H[k]$ is the channel frequency response, $S[k]$ is the transmitted frequency-domain signal, and $W[k]$ AWGN, all for subcarrier k.

Main Path Delay

If the delay spread of the multipath channel is large, received OFDM symbols may overlap; this effect is termed as inter-symbol interference (ISI). Even without ISI, the delay spread will reduce the effective CP length, affecting the sensitivity of timing synchronization. The main path delay (timing offset) usually grows with propagation distance. Assuming that the timing offset for the receiver is delayed by n_ε samples, which is equal to the actual sample n minus inaccuracy sample ε ($n_\varepsilon = n - \varepsilon$). The received samples as shown in (3-2) can be expressed as

$$r[\varepsilon] = r[n - n_\varepsilon] = \sum_i h_i[n - n_\varepsilon] \cdot s[n - n_\varepsilon - \tau_i] + w[n - n_\varepsilon] \tag{3-5}$$

Thus, we have the received signal in the frequency domain as

$$R'[k] = (H[k] \cdot S[k] + W[k]) \cdot e^{-j2\pi(k/N)\cdot n_\varepsilon} \quad \text{where N is FFT size} \tag{3-6}$$

From (3-5), we can see that the timing offset causes the phase rotation of the received signal (proportional to subcarrier index). Assuming there is no multipath fading, if the timing offset n_ε is larger than zero or smaller than the negative CP length, the inter-symbol interference (ISI) and inter-carrier interference (ICI) will occur, as depicted in Figure 3-3. For this reason, it is usually to advance a couple of samples when the timing offset is

compensated.

Fading

Multipath fading is due to the movement of the MS in NLOS environments. The mutual movement between the MS and the BS causes a shift in the carrier's frequency, called Doppler shift, as observed by the receiver. The Doppler shift varies the phase of the signal from each multipath component rapidly, resulting in the rapid change to the sum of the signals. The Doppler shift f_d can be calculated as

$$f_d = \frac{v \cdot \cos(\theta) \cdot f_c}{c} \tag{3-7}$$

,where v is the mobile's speed, θ is the angle of movement relative to the direct path between the transmitter and the receiver, f_c the carrier frequency of the system, and c the speed of light.

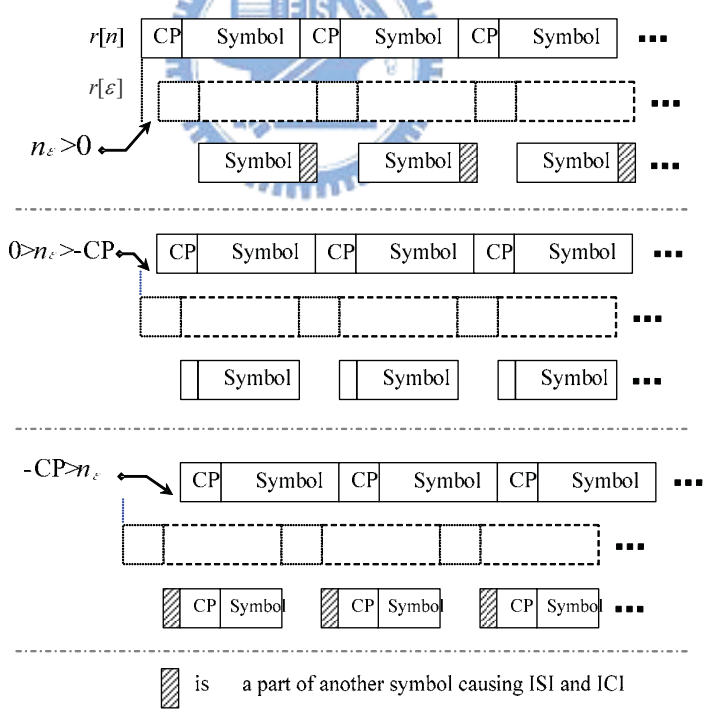

Figure 3-3 : ISI caused by timing offset

In this thesis, we adopt spatial channel model (SCM), provided by 3GPP, as our multipath channel. It provides both fixed and mobile wireless multipath fading channels. The

speed we tested in this thesis is from 20 km/h to 300 km/h.

3.2.2 Noise

Noise refers to the unwanted signals, degrading the desired signal in the system. In the communication system simulations, we often use AWGN model as the noise model. AWGN refers to additive white noise whose density function is Gaussian. It produces a simple mathematical model useful for gaining insight into the underlying behavior of a system before other phenomena can be considered. As far as the amplifier system is concerned, noise can be generated by itself and received at its input.

- Noise generated by amplifies: thermal noises, shot noise, black body radiation from the earth, and other warm objects.
- Noise received at input: atmospheric noise, man-made noise, and the inter-cell interference if the SS is on the cell boundary.

3.2.3 Inter cell interference

Segmentation in IEEE 802.16 system enhances the difficulty of preamble synchronization. As mentioned [1], [2], the preamble sequence is determined by BS's cell ID and the segment number. Figure 3-4(1) depicts one scenario in cell boundaries, in which distances from the MS to two different BS's are the same.

In this scenario, the signal sent from BS 'a' can be ignored since L may be much smaller than L_a. Figure 3-4 (2) shows another scenario that distances from the MS to all three BS's are the same. We can therefore assume that preambles received on the cell boundary have similar powers and approximate same timing offsets. Figure 3-5 shows the area where the strong inter-cell interference can exist. In these areas, the preamble synchronization will become difficult since the signal-to-noise become quit low. It is simple to see that the SNR in Figure 3-4 (1) is below 0 dB, and that in Figure 3-4 (2) is below –3 dB.

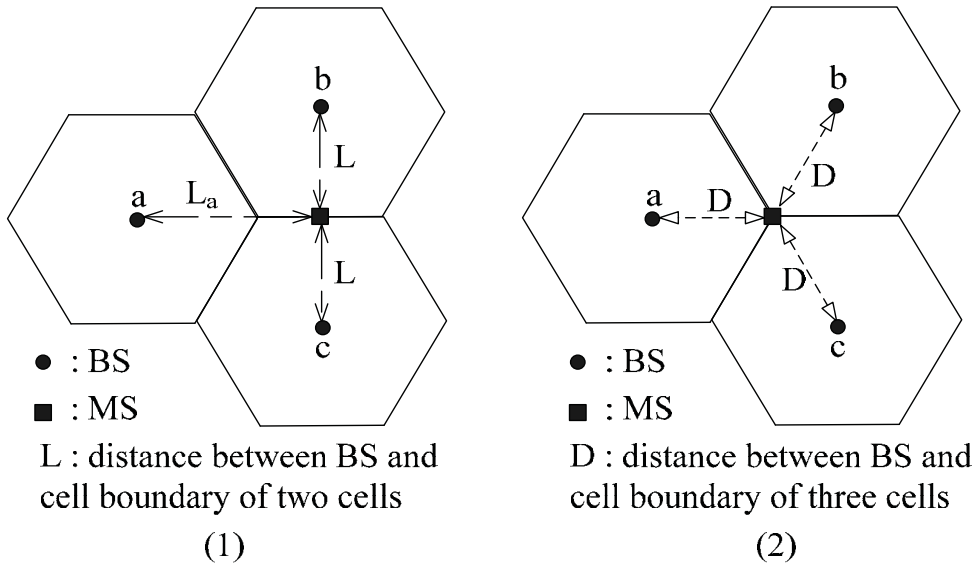

Figure 3-4: Illustration of the distance between BS and cell boundaries

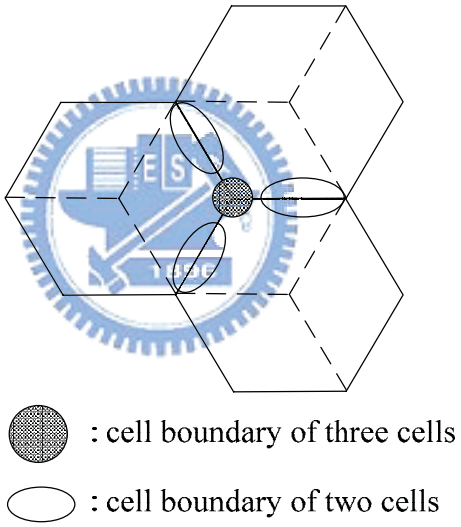

Figure 3-5: Illustration of the cell boundaries

Note that the three BS's in adjacent cells cannot be time-synchronized. As a result, preambles from different BS's will not be received at the same time slot. If the MS wants to receive the preamble signal from a certain BS, signals received from other BS's can then be considered as noise. If the BS's are synchronized, preamble signals from different BS's will be received at the same time slot. The periodical property of the preamble will be lost. In this case, preamble synchronization will not be possible.

3.2.4 Frequency Offset

Both the transmitter and the receiver use their own oscillators to generate the carrier and sampling frequencies. However, the frequencies generated in the receiver will not be exactly the same as those from the transmitter. The difference between the transmitter and receiver oscillator frequencies is called the frequency offset. The frequency offset can be divided into two types: carrier frequency offset (CFO) and sampling frequency offset (SFO).

CFO

The CFO results from the carrier frequency mismatch between the transmitter and the receiver. The OFDM systems are very sensitive to CFO, since the subcarrier spacing is very small compared to single-carrier systems. Presentation of the CFO leads to two main degradations:

1. Amplitude loss of desired subcarriers: Subcarriers are no longer sampled at the peaks of sinc-functions in the windowed DFT.
2. ICI: Sinc-functions from neighboring subcarriers are not sampled at their zero-crossings.

We abbreviate the transmitted signal $s[n]$ in (3-2) as s_n. Then, the complex passband signal can be expressed as

$$y_n = s_n \cdot e^{j2\pi \cdot f_t \cdot n \cdot t_s} \tag{3-8}$$

, where f_t is the transmitter carrier frequency. Using a carrier with frequency f_r, we can down-convert the received signal at the receiver. Let the resultant baseband signal be r_n, we then have (ignoring noise for the moment)

$$\begin{aligned} r_n &= y_n \cdot e^{-j2\pi \cdot f_r \cdot n \cdot t_s} \\ &= s_n \cdot e^{j2\pi \cdot f_t \cdot n \cdot t_s} \cdot e^{-j2\pi \cdot f_r \cdot n \cdot t_s} \\ &= s_n \cdot e^{j2\pi \cdot (f_t - f_r) \cdot n \cdot t_s} \\ &= s_n \cdot e^{j2\pi \cdot f_\Delta \cdot n \cdot t_s} \end{aligned} \tag{3-9}$$

, where $f_\Delta = f_t - f_r$ is the carrier frequency offset, $t_s = T_s / N_{FFT}$ is the sampling period. We define the normalized carrier frequency offset as

$$\psi = \frac{f_\Delta}{\Delta f} \tag{3-10}$$

, where $\Delta f = F_s / N_{FFT}$ is the subcarrier spacing. We further split the normalized CFO into

$$\psi = z + \delta \qquad , z \in \mathbb{Z}, |\delta| < 1 \tag{3-11}$$

, where z is the integral part of the CFO (ICFO), and δ is the fractional part of the CFO (FCFO). Generally, we have to deal with both ICFO and FCFO.

SFO

The SFO results from the mismatch between the frequency used in the digital to analog converter (DAC) at the transmitter, and that in the analog to digital converter (ADC) at the receiver. The SFO will have two main effects:

1. A slow drift of the symbol timing boundary, which rotates the phase of the subcarriers similar to timing offset

2. Loss of the orthogonality of the subcarriers, leading to ICI and loss of signal to noise ratio (SNR)

Let the SFO be $\Delta T = T' - T$ where T' and T are the receiver and transmitter sampling periods, respectively, as shown in Figure 3-6. Then the normalized sampling error can be defined as $t_\Delta = \frac{T' - T}{T}$. After DFT, the received signal can be expressed as

$$R_l[k] = e^{j2\pi \cdot k \cdot t_\Delta \cdot l \cdot \frac{T_s}{T_u}} \cdot S_l[k] \cdot \mathrm{sinc}(\pi \cdot k \cdot t_\Delta) \cdot H_l[k] + W_l[k] + C(t_\Delta)_l[k] \tag{3-12}$$

, where l is the OFDMA symbol index, k is the subcarrier index, T_s is the duration of the total symbol, T_u is the duration of the useful data portion, W_l is AWGN and $C(t_\Delta)_l$ is the induced

ICI due to the SFO.

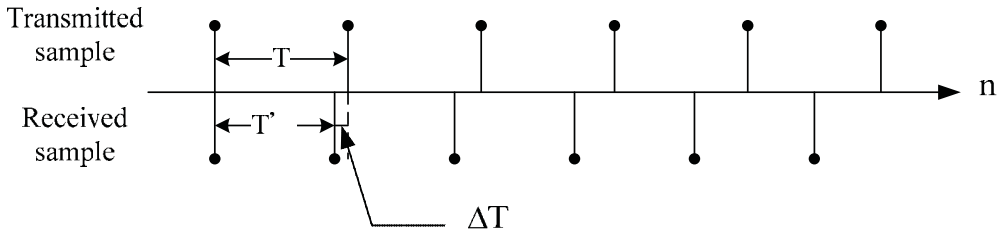

Figure 3-6: Transmit and receive sampling periods

Figure 3-7 shows an example comparing the original symbol waveform and that affected by SFO. We can see that even the SFO is comparatively small, it still can cause a significant deviation after a long period time.

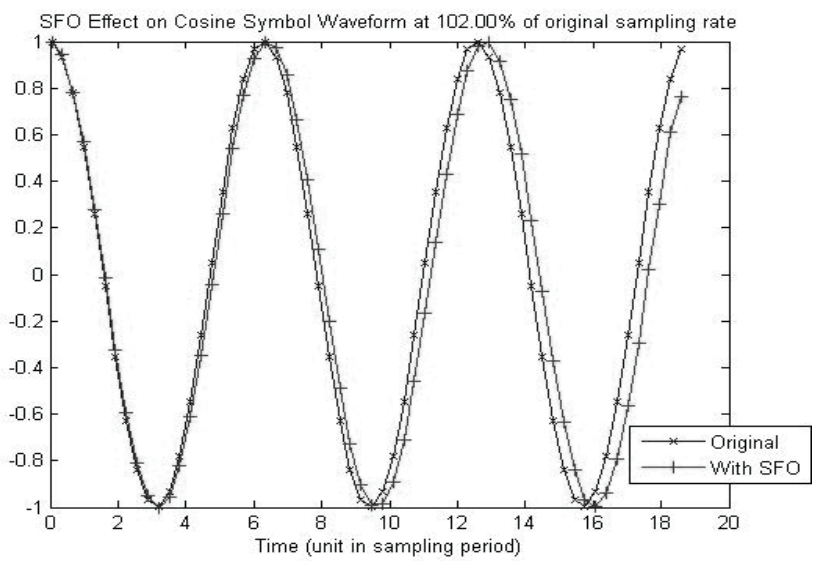

Figure 3-7 : SFO in cosine function

If the ΔT is small enough that the ICI term can be ignored, the remained significant term is $e^{j2\pi \cdot k \cdot t_{\Delta} \cdot l \frac{T_s}{T_u}}$. This term shows the amount of angle rotation experienced by the different subcarriers, as shown in Figure 3-8. The angle depends on both the subcarrier index *k* and the OFDMA symbol index *l*. Even though the term ΔT is quite small, as *l* increases, the rotation may eventually become so large that correct demodulation is no longer possible.

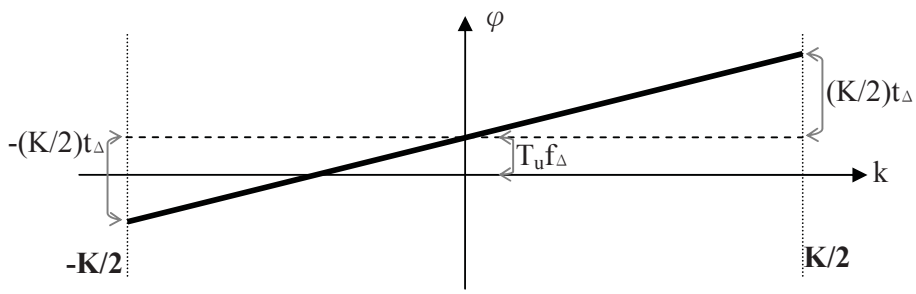

Figure 3-8 : SFO effect in the frequency domain

3.3 Proposed Inner Receiver Design

The preamble search method used in [7] is to choose the preamble sequence, having the maximum correlation value with the received preamble. This is considered as the conventional preamble search method in this thesis.

In [8], an inner receiver design for the IEEE 802.16e OFDMA system was proposed. In this work, CFO was assumed to be less than half of the tone spacing. However, from the oscillator precision defined in IEEE802.16, we can know that CFO can be larger than half the tone spacing and even ICFO can occur. Note that the CFO estimation problem is complicated by the spectrum segmentation. In a no-CFO scenario, CFO estimate for the segment-1 preamble and the segment-2 preamble will be one and two tone spacing, respectively. Thus, for an estimated CFO, there is no way to tell if that is a true CFO or not. Due to this problem, the preamble search and CFO estimation should be considered simultaneously.

In [6], another inner receiver design was also proposed. It conducts the preamble search with the Kronecker product of the known preamble sequence and the received preamble. However, it still requires many FFTs, and complex multiplications. In the following subsections, we will propose a low-complexity inner receiver design remedying the problem mentioned about.

3.3.1 Packet Detection

Packet detection is to find an approximate estimate of the start of the preamble of an incoming data packet. It is the first synchronization algorithm that must be performed in the inner receiver. The rest of the synchronization process is highly dependent on the packet detection result. There are two performance indexes in packet detection. If a packet has actually arrived and not detected, it is called missing. If no packet has arrived but been detected, we call it false alarm. Generally, a false alarm is a less severe event than a missing, since the missing always results in data lost. Thus, we also consider it as a packet detection error.

The preamble of the IEEE 802.16e OFDMA has been designed with a repeated structure. Here, we use a well-known method called: "delay, correlated and normalized detection (DCND)" [10]. Define three variables c_n , e_n , and m_n as:

$$c_n = \sum_{k=0}^{L-1} r_{n+k} \cdot r_{n+k+D}^{*} \tag{3-13}$$

$$e_n = \frac{1}{2} \cdot \sum_{k=0}^{L-1} \left(r_{n+k} \cdot r_{n+k}^{*} + r_{n+k+D} \cdot r_{n+k+D}^{*} \right) = \frac{1}{2} \cdot \sum_{k=0}^{L-1} \left(\left| r_{n+k} \right|^2 + \left| r_{n+k+D} \right|^2 \right) \tag{3-14}$$

$$m_n = \frac{\left| c_n \right|^2}{\left(e_n \right)^2} \tag{3-15}$$

The delay D in above equations is equal to the period of the preamble. There are two windows called C and E and the window length is L. The C window calculates a sequence of the crosscorrelation c_n between the received signal and its delayed version (delay and correlate). The E window calculates the received signal energy for the crosscorrelation window. The value of the E window is then used to normalize the decision statistic, so that the value of the decision statistic is not dependent on the absolute received power level. When the decision variable m_n exceeds a predefined threshold, a detected packet is claimed. As discussed, the preamble of the IEEE 802.16e system has a period of $D = floor(2048/3) = 682$,

the one third of the preamble symbol. Her, we set $L = 64$ in (3-13) and (3-14) for the low-complexity consideration. The operation of the algorithm is shown in Figure 3-9.

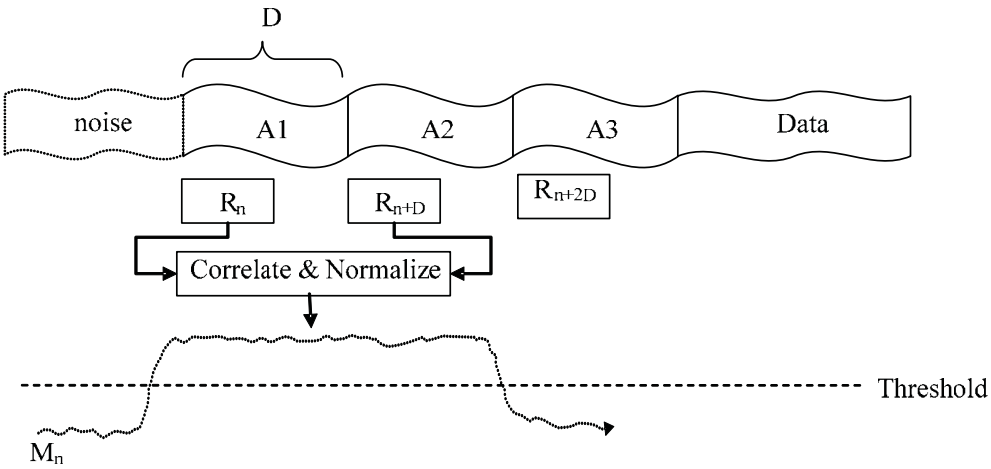

Figure 3-9: Delay, correlated and normalized detection algorithm

Figure 3-10 illustrates an example of the decision statistic for the preamble. Note that the normalized decision variable is restricted between [0,1] and the start of the packet can be seen very clearly. When the received signal consists of noise only, c_n is a zero-mean random variable. This explains the low level of m_n before the start of the packet. Once a packet is received, c_n corresponds to a crosscorrelation of two identical preambles. Thus, m_n jumps up quickly to its maximum value. For low SNR environments, m_n may have its maximum before or after the start of the real packet. To increase the detection reliability, we add a sliding window W and conduct further processing using m_n in the window. Two thresholds are defined; the first one is for m_n and the other is for the number of m_n exceeding the first threshold in the window. If the number of m_n in the window being higher than the first threshold is higher than the second threshold (may be three forth), a detected packet is claimed. The rationale for this approach is that if a packet actually arrives, the decision statistics m_n will remain high until the end of the preamble period. This is a modification mentioned in [7]. In low SNR environments, we adjust the length of the window w, shown in Figure 3-10, to be $L_w = 50$, the first threshold to be 0.5, and the second threshold to be

3/5L. With these parameters, we can have a good tradeoff between performance and computational complexity.

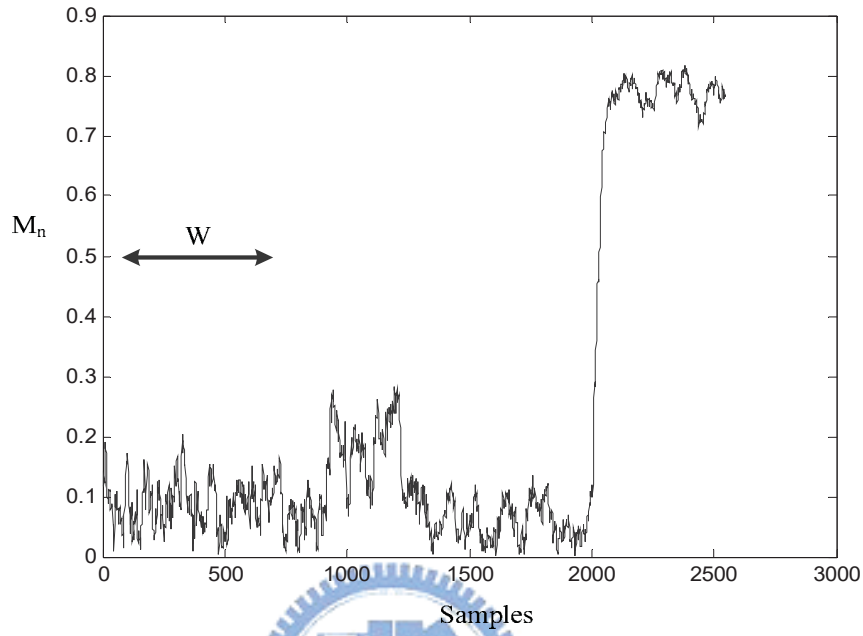

Figure 3-10: Response of the packet detection

3.3.2 Frequency Synchronization

One of the main drawbacks of OFDM is its sensitivity to CFO. The effect has been outlined in Section 3.2.3. We split the actual normalized CFO as shown in (3-11) into ICFO and FCFO. In our processing, we will first estimate FCFO and compensate for its effect. After the preamble search is completed, we exploit the estimated segment number to determine ICFO.

In the literature, many algorithms have been developed to estimate the CFO in OFDM systems [10]. One data-aided algorithm, exploring the periodic property of the preamble, allows the receiver to have the maximum likelihood estimate of the CFO. The method that operates on the time domain signal has been presented in several papers such as [11]. It requires at least two consecutive repeated OFDM symbols. As described in Section 3.1, the preamble of IEEE 802.16 has three approximately identical periods. Thus, the ML method is

then applicable. We now develop the FCFO estimator as follows.

Let D be the delay between the identical samples of the two repeated symbols and define an intermediate variable u as

$$\begin{aligned} u &= \sum_{n=0} r_n \cdot r^*_{n+D} \\ &= \sum_{n=0}^{L-1} s_n \cdot e^{j2\pi \cdot f_\Delta \cdot n \cdot t_s} \cdot \left(s_{n+D} \cdot e^{j2\pi \cdot f_\Delta \cdot (n+D) \cdot t_s} \right)^* \\ &= \sum_{n=0}^{L-1} s_n \cdot s_{n+D} \cdot e^{j2\pi \cdot (n-n-D) \cdot f_\Delta \cdot t_s} \\ &= e^{-j2\pi \cdot D \cdot f_\Delta \cdot t_s} \cdot \sum_{n=0}^{L-1} \left| s_n \right|^2 \end{aligned} \tag{3-16}$$

where L is the window length of the estimator. The CFO can then be estimated as

$$\hat{f}_\Delta = -\frac{\angle u}{2\pi D t_s} \tag{3-17}$$

Since the sampled preamble does not have exact three periods, we cannot find an integer D between identical samples. Note that the ideal delay D' is $682\,1/3$. Thus, we can consider a linear interpolation to interpolate $r_{n+D'}$. Then,

$$\begin{aligned} u &= \sum_{n=0}^{L-1} r_n \cdot r^*_{n+682\,1/3} \\ &= \sum_{n=0}^{L-1} r_n \cdot \left(\frac{1}{3} r^*_{n+682} + \frac{2}{3} r^*_{n+683} \right) \\ &= \frac{1}{3} \sum_{n=0}^{L-1} r_n \cdot r^*_{n+682} + \frac{2}{3} \sum_{n=0}^{L-1} r_n \cdot r^*_{n+683} \end{aligned} \tag{3-18}$$

A limitation of the CFO estimation method is its operation range, which defines how large the CFO can be estimated. The range is directly related to D'. Note that $\angle u = -2\pi \cdot D' \cdot f_\Delta \cdot t_s$, which is unambiguous only in the range [$-\pi$, π]. Thus if the absolute value of the CFO is lager than the limit shown below, the result will be incorrect.

$$\left| f_\Delta \right| \geq \frac{\pi}{2\pi D' t_s} = \frac{1}{2D' t_s} \tag{3-19}$$

Since the subcarrier spacing can be represented as

$$\begin{aligned}\Delta f &= \frac{F_s}{N_{FFT}} \\ &= \frac{1}{t_s \cdot N_{FFT}}\end{aligned} \tag{3-20}$$

The maximum CFO that can be estimated will be

$$\left|f_{\Delta\max}\right| \geq \frac{1}{2D't_s} = \frac{N_{FFT}\cdot\Delta f}{2D'} = \frac{N_{FFT}\cdot\Delta f}{2\frac{N_{FFT}}{3}} = 1.5\Delta f \tag{3-21}$$

For Mobile WiMAX, the channel bandwidth for FFT size 2048 is 20 MHz, $f_{\Delta\max} = 14.65$ KHz. The maximum CFO range can be estimated becomes $\pm 1.5\Delta f$. The maximum CFO tolerated range for this method is $\left[-1.5\Delta f, 1.5\Delta f\right]$. However, from the required precision of the oscillator, we can calculate that the possible CFO is from $-3.5\Delta f$ to $3.5\Delta f$. Thus, the ICFO estimation is required. We will leave this problem after the preamble search is completed.

3.3.3 Preamble Series Search

Different from the OFDM mode, the OFDMA mode has multiple preamble series. The BS determines the preamble series by the segment number and ID cell. Not until the preamble is received, does the receiver knows which preamble series was transmitted. The receiver has no priori information regarding the preamble series it will receive. As a result, it has to search the most likely one from 114 possible preambles.

Since the preamble series is BPSK-modulated in one-third of subcarriers, Let the modulated preamble subcarriers (excluding guard bands) be denoted as

$$P[k] = \begin{cases} \{1, -1\}, & when \quad k = 3v + s \\ 0, & otherwise \end{cases} \tag{3-22}$$

where $P[k]$ is the preamble subcarrier, k is the useful subcarrier index from 0 to 1703, v

is the running index from 0 to 567 (568 is the length of the preamble series), and s is the segment number, being equal to 0, 1 and 2.

The received preamble subcarriers can be written as

$$\begin{aligned} R[k] &= P[k]\cdot H[k]+W[k] \\ &= \begin{cases} P[3v+s]\cdot H[3v+s]+W[3v+s], & when\ k=3v+s \\ W[k] & ,otherwise \end{cases} \end{aligned} \tag{3-23}$$

where $H[k]$ is the channel response, $W[k]$ is the AWGN.

For simplicity, we will neglect the noise but only consider the each third preamble subcarriers with value as

$$\begin{aligned} \tilde{R}[v] &= R[3v+s], \qquad v=0,1,\ldots,567 \\ &= \tilde{P}[v]\cdot\tilde{H}[v]+\tilde{W}[v] \\ &= P[3v+s]\cdot H[3v+s]+W[3v+s] \end{aligned} \tag{3-24}$$

where ~ represents the each third preamble subcarriers.

3.3.3.1 Conventional Preamble Search Method

The conventional preamble search method is to correlate the received preamble subcarriers with all the preamble series in the frequency domain. Note that the correlation in the time domain is equivalent to the multiplication in the frequency domain. To do that, the received preamble must first be transformed to the frequency domain (with DFT), multiplied by the conjugate of the possible preamble series, and then transformed back to the time domain (with IDFT). Figure 3-11 shows the result of one example. The one with the largest magnitude is then outputted as the desired preamble series index.

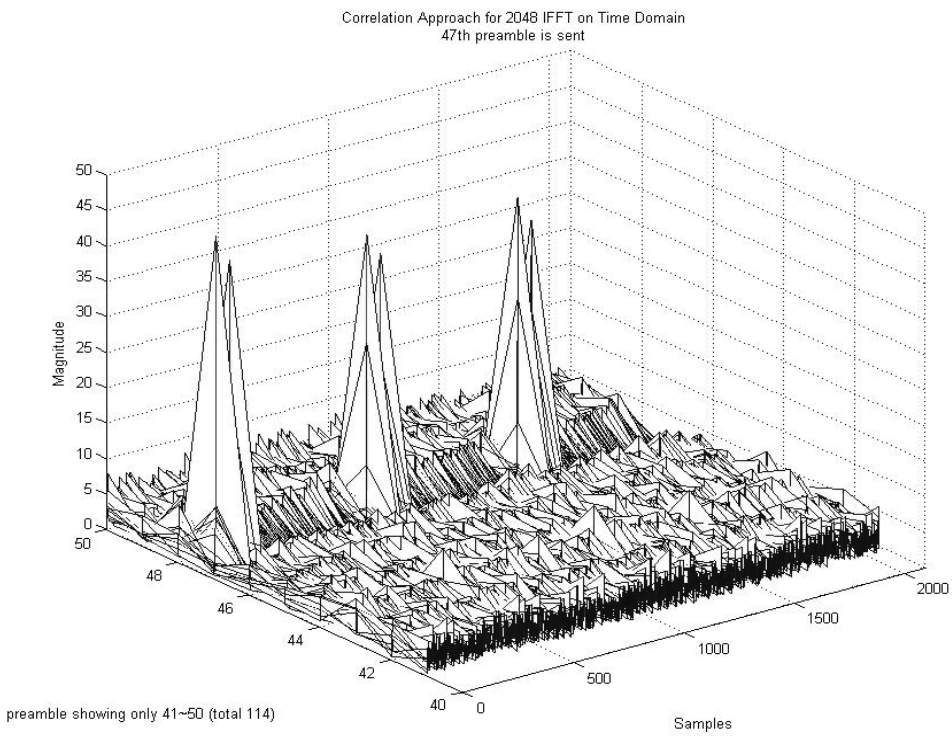

Figure 3-11: Correlation result in time domain

The conventional approach requires a lot of complex number multiplications and FFT operations. The algorithm of the conventional approach can be written as

$$\hat{m} = \arg \max_{m=0,\ldots,113} \left| IDFT\{\left(\tilde{R}[k] \cdot \tilde{P}_m[k]\right)\} \right|^2 \tag{3-25}$$

where $\tilde{P}_m[v]$ is the specified preamble series with index m from 0 to 113. As we can see from the structure in Figure 3-12, it requires a high computational complexity. In what follows, we will propose a low-complexity preamble search algorithm.

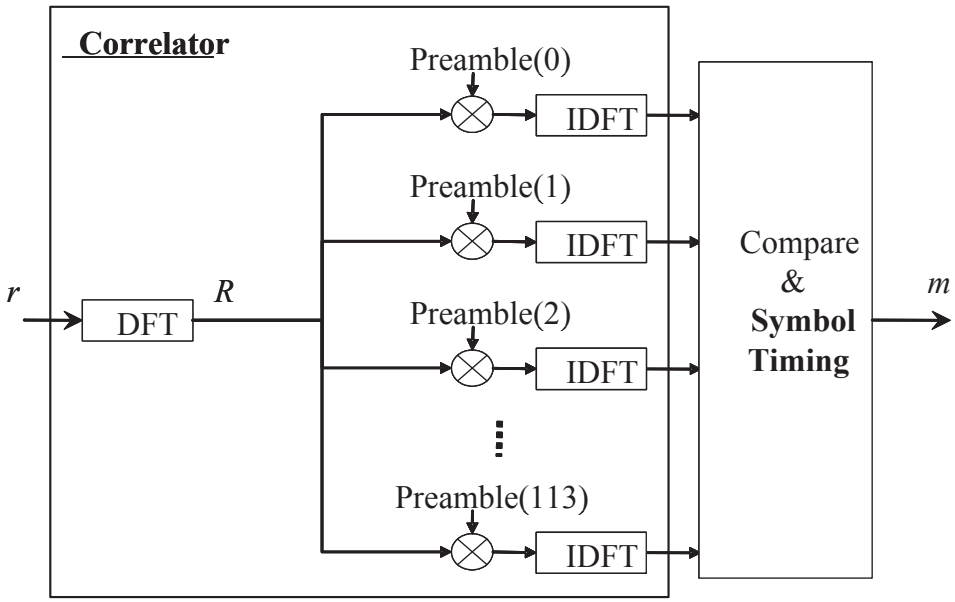

Figure 3-12: Structure of conventional preamble search algorithm

3.3.3.2 Proposed Preamble Search Method

For a low-complexity preamble search algorithm, the following properties are desired.

- All the operations must be conducted in the frequency domain. The preamble series are binary sequences in the frequency domain, and the corresponding processing is much easier than that in the time domain.
- Only simple operations, such as additions and comparisons are required.
- Major operations can be shared for testing a set of series.
- It is not necessary to use the whole length of the series, which is 568. A smaller number should be sufficient.

The first step is to multiply the received signal in (3-24) by a possible preamble series. Since the channel response is unknown, the next step is to remove the channel effect. Specifically, we propose to apply the differentiation operation on the series-matched signal. It leads to the following observation.

- If the series is correct, the matched result will just contain noise, which is small after differentiation.
- If not, the matched result is a random sequence, which will be large after differentiation.

Figure 3-13 illustrates the differential result of the preamble signal is matched; it is just a null signal.

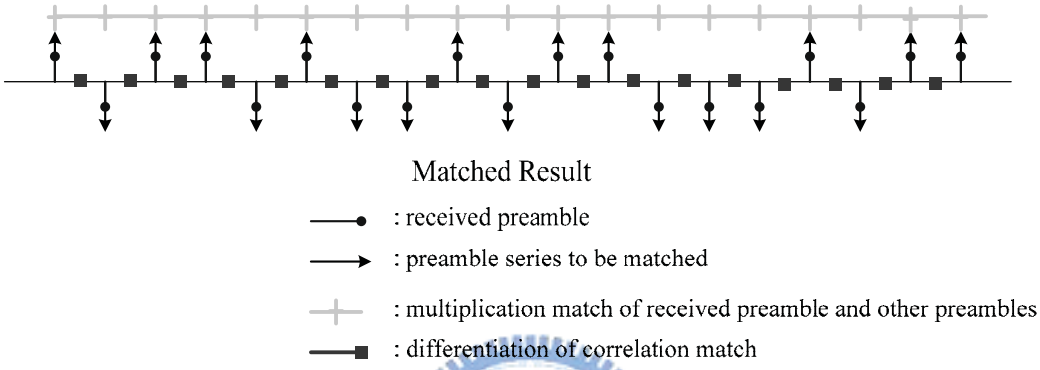

Figure 3-13: Differentiation of matched result (code-matched case)

Figure 3-14 illustrates the result if the received preamble is not matched. As we can see, the results will be non-zero.

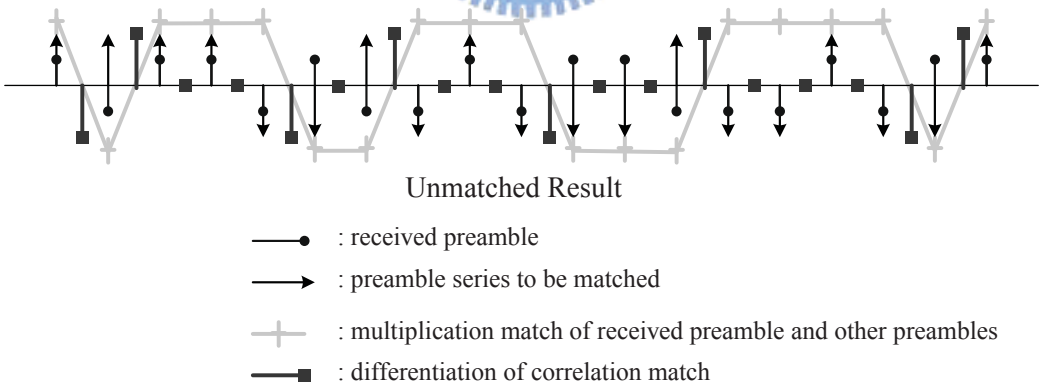

Figure 3-14: Differentiation of matched result (code-unmatched case)

Using the idea, we then develop our algorithm. Let the received signal after preamble matching is expressed as

$$
\begin{aligned}
\tilde{M}[v] &= \tilde{P}_m[v]\cdot\tilde{R}[v] \qquad\qquad ,m=0,\ldots,113 \\
&= \tilde{P}_m[v]\cdot\tilde{P}[v]\cdot\tilde{H}[v]+\tilde{P}_m[v]\cdot\tilde{W}[v] \\
&= \begin{cases} \tilde{H}[v]+\tilde{P}_m[v]\cdot\tilde{W}[v], & \text{if matched} \\ -\tilde{H}[v]+\tilde{P}_m[v]\cdot\tilde{W}[v], & \text{if unmatched} \end{cases}
\end{aligned} \tag{3-26}
$$

where $\tilde{P}_m[v]$ is the candidate preamble sequence. Here, we assume that the coherent bandwidth is much larger than the tone spacing such that the channel response can be considered as constant in a couple of consecutive tones. As a result, the differential operation can remove the unknown channel effect. Let the channel response can be approximated as

$$
\tilde{H}[v+1]=\tilde{H}[v] \tag{3-27}
$$

We also assume that the noise level is small compared to the signal amplitude such that it can be ignored.

$$
\tilde{W}[v]=0 \tag{3-28}
$$

Applying (3-27) and (3-28) in two adjacent preamble subcarriers, and taking the absolute value of the differential result, we have

$$
\begin{aligned}
\left|\tilde{D}[v]\right| &= \left|\tilde{M}[v+1]-\tilde{M}[v]\right| \\
&= \left|\tilde{P}_m[v+1]\cdot\tilde{P}[v+1]\cdot\tilde{H}[v]-\tilde{P}_m[v]\cdot\tilde{P}[v]\cdot\tilde{H}[v]\right| \\
&= \begin{cases} 0, if \begin{cases} \left(\tilde{P}[v+1]=\tilde{P}_m[v+1]\right) \ \& \ \left(\tilde{P}[v]=\tilde{P}_m[v]\right) \\ \left(\tilde{P}[v+1]=-\tilde{P}_m[v+1]\right) \ \& \ \left(\tilde{P}[v]=-\tilde{P}_m[v]\right) \end{cases} \\ \left|2\tilde{H}[v]\right|, \qquad\qquad otherwise \end{cases}
\end{aligned} \tag{3-29}
$$

Equation (3-29) indicates that there are two possible results for the adjacent two bits. Then, if we assume $(\tilde{P}[v+1],\tilde{P}[v])=(1,1)$, $\left|\tilde{D}[v]\right|$ has two different values as

$$\begin{cases} \left|\tilde{D}[v]\right| = 0. & \text{, if } \begin{cases} (\tilde{P}_m[v+1], \tilde{P}_m[v]) = (1,1) \\ (\tilde{P}_m[v+1], \tilde{P}_m[v]) = (-1,-1) \end{cases} \\ \left|\tilde{D}[v]\right| = \left|2\tilde{H}[v]\right|. & \text{, if } \begin{cases} (\tilde{P}_m[v+1], \tilde{P}_m[v]) = (1,-1) \\ (\tilde{P}_m[v+1], \tilde{P}_m[v]) = (-1,1) \end{cases} \end{cases} \tag{3-30}$$

So, after finishing the differentiation of the whole preamble sequence, we can obtain the most likely preamble series index by choosing the minimum sum of $\left|\tilde{D}[v]\right|$ from each preamble series.

Observing (3-29), we can find that there is an easier way to find the minimum. There is no need to try all the preamble sequences. We can first convert the received signal into a binary sequence since there are only two possible results in the differential operation in (3-29).

$$B[o] = \begin{cases} 0, if \ (\tilde{P}[v+1], \tilde{P}[v]) = (1,1) \text{ or } (-1,-1) \\ 1, if \ (\tilde{P}[v+1], \tilde{P}[v]) = (1,-1) \text{ or } (-1,1) \end{cases} \tag{3-31}$$

Thus, each pair of two bits requires only two additions to obtain the binary sequence.

$$B[o] = \arg\min_{q=0,1} \left(\left| \tilde{R}[v+1] \cdot (-1)^q - \tilde{R}[v] \right| \right) \tag{3-32}$$

We also convert all the 114 preamble series to binary sequences using the same rules.

$$B_m[o] = \begin{cases} 0, if \ (\tilde{P}_m[v+1], \tilde{P}_m[v]) = (1,1) \text{ or } (-1,-1) \\ 1, if \ (\tilde{P}_m[v+1], \tilde{P}_m[v]) = (1,-1) \text{ or } (-1,1) \end{cases}, o = 1, \ldots, L_{diff} \tag{3-33}$$

Since $B[o]$ and $B_m[o]$ are all binary sequences, we can then use simple operations such as XORs, adders and registers to find the most likely $B_m[o]$ matching $B[o]$.

$$\hat{s} = \arg\min_m \sum_o \left\{ XOR(B_m[o], B[o]) \right\} \tag{3-34}$$

Figure 3-15 shows the hardware implementation of the proposed preamble search scheme. The minimum value among the results of XOR is the desired preamble series.

For the preamble length of 568 (FFT size 2048), the length of differentiation is 567. We

can see from Figure 3-14 that each mis-matched subcarrier will cause two non-zero results. We consider two bits as a unit for differentiation andd convert the whole 568 bits into 284 clips. Furthermore, we only have to distinguish 114 preamble sequences which are much smaller than the combinations of 568 bits. Thus, not all bits are required to be used. Let the length of the differentiated sequence be L_{diff} (the number of clips) and $L_{diff} < 284$. We will see that the value of L_{diff} can be quite small.

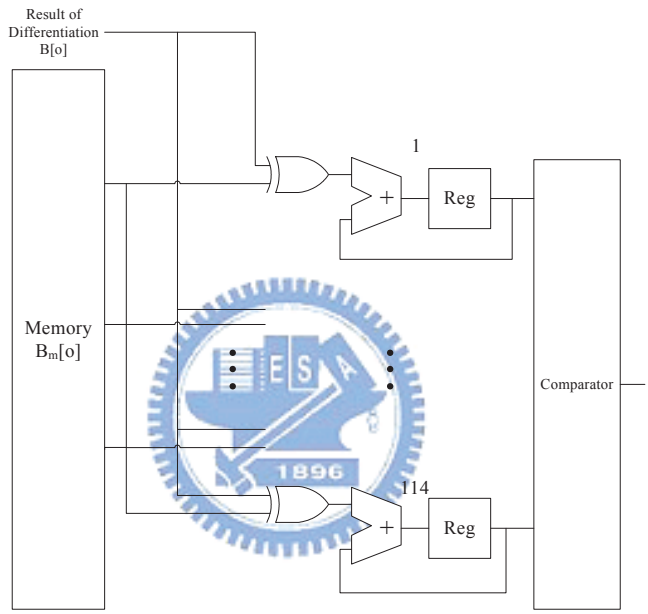

Figure 3-15: Hardware implementation of proposed approach

For the proposed method shown above, it is simple to see that the required computational complexity is reduced to $114 \times L_{diff}$ XOR operations and $(2L_{diff} + 114 \times L_{diff})$ additions (differentiations and accumulations). Note that the key to the low-complexity algorithm is that we do not have to exactly match the whole preamble sequence, only most of it is sufficient. This is the reason why only two conditions has to be checked in (3-31) and (3-33).

Table 3-1: Computational Complexity Comparison of conventional approach and proposed approach

	FFT		Complex multiplication	Complex addition
	$O(N\log_2 N)$	N=2048	$N_p = 568$	$N_p = 568$
Conventional approach in [6]	114		$114 \times N_p$	0
DS-WS approach in [8]	114		$114 \times \frac{N_p}{3}$	$\frac{114}{3} \times \frac{N_p}{3} + N_p$
DS-WOS approach in [8]	1		$114 \times N_p$	$114 \times N_p$
Proposed approach	1		0 (XOR)	$(2L_{diff} + 114 \times L_{diff})$

Table 3-1 compares the computational complexity of the conventional and the proposed preamble sequence search algorithms. It is apparent that that the complexity of the proposed approach is significantly lower than the conventional approach in [6] and that in [8]. Also, the hardware architecture for the proposed algorithm is much simpler. Note that the DS-WS approach in [8] and the preamble search approach used in [7] both assume there is no ICFO. The DS-WOS approach in [8] is developed to overcome the problem.

3.3.4 ICFO Compensation

If we can identify the correct preamble series, we know the segment number of the preamble. Then, we know the original subcarrier positions carrying the preamble data. After the FCFO is estimated, we conduct the compensation for the input signal. Thus, only ICFO is remained. Note that the deviation of the received preamble subcarriers from the original subcarrier positions is the ICFO (a multiple of subcarrier spacing).

$$\sum_{v=0}^{567}\left|R[3v+s+\psi]\right|^2 \tag{3-35}$$

where ψ is the ICFO.

To find the deviation, we can first set a sliding window with the size of the useful subcarriers, and find the position which gives the minimum result of (3-34)

$$E_R[d]=\sum_{v=0}^{567}\left|R[3v+d]\right|^2, d=-3\sim 5 \tag{3-36}$$

where $d=0,1,2$ corresponds to the original position that segment 0, 1, 2 starts. If we want to have a better result, the search area can be enlarged. Denote the resultant d as d_{max}. Then, we let $R[3v+d_{max}]$ as the received signal in (3-23).

$$\hat{R}[v]=R[3v+d_{\max}] \tag{3-37}$$

After the preamble search is completed, the ICFO can then be found from the difference of the deviation and the estimated segment number $\hat{s}$ in (3-34) as

$$\hat{\psi}=\hat{s}-d \tag{3-38}$$

Once we have found the ICFO, we can include it in the CFO compensation, which is

$$\begin{aligned} r_n'' &= r_n' \cdot e^{-j2\pi\cdot\hat{z}\cdot\Delta f\cdot n\cdot t_s} \\ &= \left(r_n \cdot e^{-j2\pi\cdot\hat{\delta}\cdot\Delta f\cdot n\cdot t_s}\right)\cdot e^{-j2\pi\cdot\hat{z}\cdot\Delta f\cdot n\cdot t_s} \\ &= r_n \cdot e^{-j2\pi\cdot\left(\hat{\delta}+\hat{z}\right)\cdot\Delta f\cdot n\cdot t_s} \\ &= r_n \cdot e^{-j2\pi\cdot\hat{\psi}\cdot\Delta f\cdot n\cdot t_s} \\ &= s_n \cdot e^{j2\pi\cdot(f_\Delta-\hat{\psi}\cdot\Delta f)\cdot n\cdot t_s} \end{aligned} \tag{3-39}$$

where r_n' is the FCFO-compensated received preamble symbol, r'' is the ICFO-compensated received preamble symbol. A good estimate of FCFO and ICFO will lead to

$$f_\Delta-\hat{\psi}\cdot\Delta f\approx 0 \tag{3-40}$$

3.3.5 Symbol Timing Offset Estimation

The objective of symbol timing offset (STO) estimation is to locate the edge of an OFDM symbol. The result is used to define the DFT window, a set of samples for the DFT operation. Since the preamble is available to the receiver, it enables the receiver to use the simple correlation-based STO algorithm. After the packet is detected, the start of the packet is roughly located. The STO refines the precision to the sample-level. Thus, the packet detection can be regarded as a coarse symbol timing synchronization, and the symbol timing correction as a fine symbol timing synchronization.

As mentioned, we use the correlation-based algorithm expressed as follows

$$\hat{t}_{STO} = \arg\max_{l} \left| \sum_{n=0}^{L-1} r_l[n] \cdot p[n] \right|^2 \tag{3-41}$$

where $r_l[n]$ is the received preamble and $p[n]$ is the known preamble. The value of l corresponding to the maximum absolute value of the correlation is the STO estimate $\hat{t}_{STO}$ and the L is the length of the correlated window.

Note that the correlation operation for the STO estimation has been completed in the preamble series search. We need only to transform the matched preamble back to the time domain. The receiver can then determines the sample index l corresponding to the maximum value of the time domain signal.

3.3.6 Channel Estimation

The IEEE 802.16e system provides the preamble symbol and pilots for channel estimation. Since the number of known subcarriers in the preamble is large (568), its estimation accuracy is better. But due to the time-variant characteristic of the channel and the large frame size (48 OFDMA symbols in 5ms frame), the channel estimate may only be useful for recovering the data in FCH and DL-MAP.

The channel estimate with pilots is less accurate since the number of pilots inserted in OFDMA symbols is limited. The insertion of pilots makes it capable of tracking the channel variation, phase noise, and SFO. Since the signal in the preamble and the pilots are not placed on all subcarriers, interpolation is then required. The pilot location of the cluster/tile can be seen in Figure 2-9 and Figure 2-10. The STC scheme requires MISO channel estimation, which is allowed by splitting some pilots between the 2 Tx antennas, as shown in Figure 2-15. The received preamble or pilots can be expressed as

$$R_q[k] = H_q[k] \cdot X_q[k] + W_q[k] \tag{3-42}$$

where $H_q[k]$ is the channel response, $X_q[k]$ is the transmitted known data, $W_q[k]$ is AWGN, all for the kth subcarrier and the qth symbol. The channel estimation can be calculated as

$$\begin{aligned} \hat{H}_q &= R_q \cdot X_q^* \Big/ \left|X_q\right|^2 \\ &= \left(H_q \cdot X_q + W_q\right) \cdot X_q^* \Big/ \left|X_q\right|^2 \\ &= \left(H_q \cdot \left|X_q\right|^2 + W_q \cdot X_q^*\right) \Big/ \left|X_q\right|^2 \\ &= H_q + W_q \cdot \frac{X_q^*}{\left|X_q\right|^2} \end{aligned} \tag{3-43}$$

For low to moderate mobile speed, the interpolation can achieve satisfactory results. However, for high-speed mobile environments; however, straightforward interpolation may not meet the requirement. A simple and effective interpolation scheme has been developed in [12]. In this thesis, we will use the method to conduct channel estimation. For details, please see [12].

Chapter 4: Simulation Results

In this chapter, we conduct simulations to evaluate the performance of the designed inner receiver, and that of the uplink/downlink OFDMA transceiver. We will first evaluate the performance of the proposed preamble search algorithm. Then, we analyze how well the CFO and SFO are estimated. Finally, we give the result of the DL receiver (with STC), and that of the UL receiver. The bit-error-rate (BER) is used as the performance index, and the result under various impairments such as AWGN, multipath channel fading, CFO, and SFO will be provided. The FFT size is set as 2048.

We choose Urban macro-cell as the channel type in the SCM model. The cell coverage is 1~6 km. The BS antenna is set above rooftop height, ranging from 10m to 80m. The average height is 32 m. The MS's mobile speed is between 0~250 km/hr. There are 6 taps (paths) in the channel impulse response, and the channel length is under 150 samples. The channels are all assumed to be quasi-stationary. Also, we assume that there are two MSs in the cell.

4.1 Preamble Search

This scenario is designed to evaluate the performance of the preamble search. Here, we consider only the effect of multipath channel fading and AWGN, assuming perfect timing and CFO estimation. Thus, there are only two operations in the simulation: packet detection and preamble search. Note that the performance index consider here is the rate of the preamble decision error.

The worst case for a MS is to perform a preamble search when it is in the cell boundaries. As mentioned in Section 3.2.3, the SNR will be as low as -3dB. The maximum differentiation length L_{diff} is set as 280. Figure 4-1 shows the simulation results. From Figure 4-1, we can see that for $L_{diff} = 70 \sim 280$, all results are similar. Also, the error rate is very small (cannot

show in the figure) when SNR=-3 dB. Even for L_{diff} =50, the error rate is still small. Note that if the SNR is too low, the system performance will be dominated by the packet detection, not the preamble search. We can then conclude that it is sufficient to let L_{diff} =50.

Figure 4-2 gives the comparison of the false preamble detection probability for the proposed approach and the DS-WOS approach in [8]. The channels used are generated from the non-stationary SCM model. We can see that the proposed approach is slightly better than the DS-WOS approach. The differentiation length used here is 567.

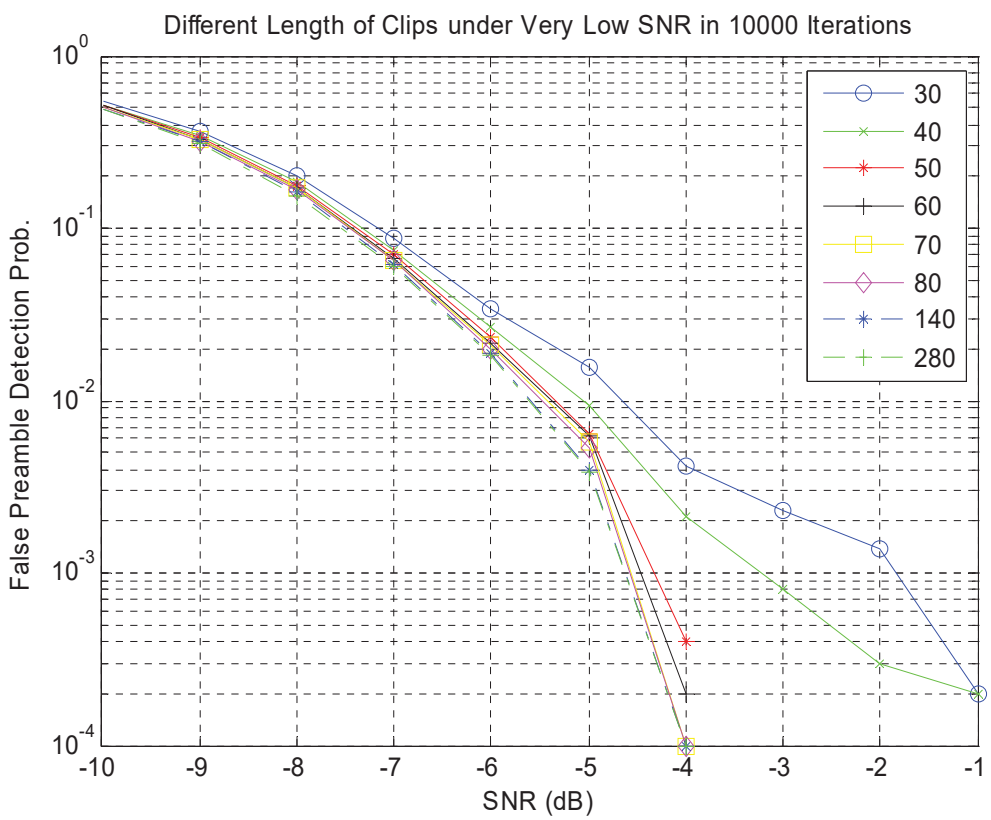

Figure 4-1: False preamble detection probability of preamble search; quasi-stationary SCM channel, 2048 subcarriers, mobile speed 100~200 km/h

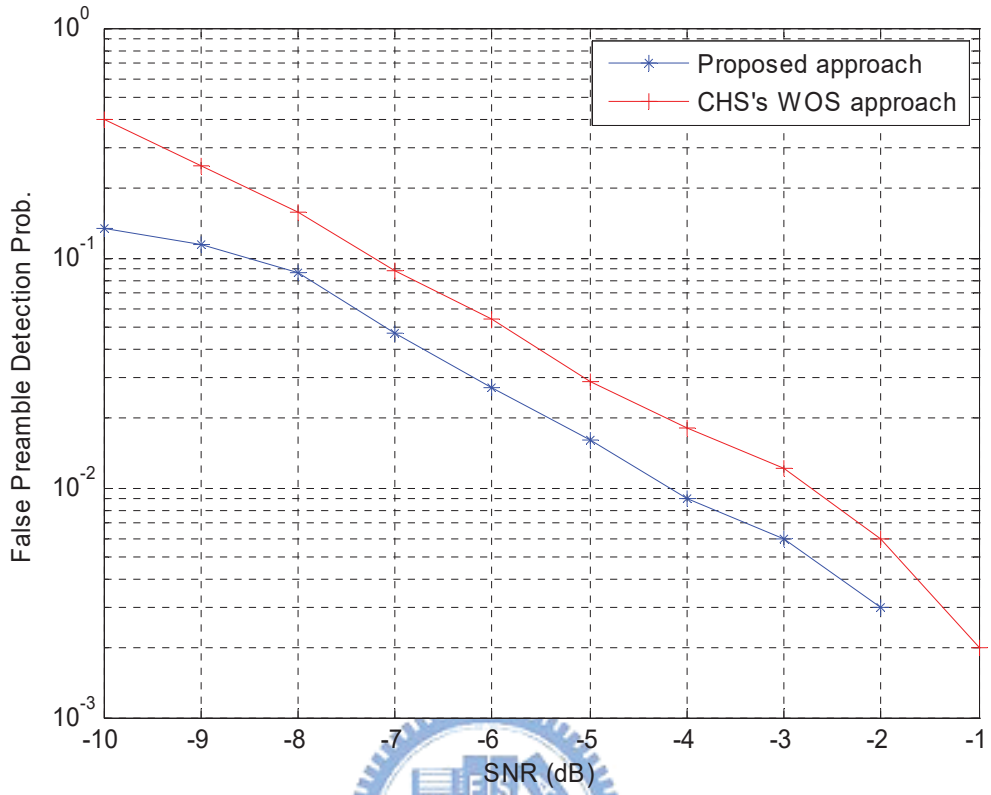

Figure 4-2: False preamble detection probability of preamble search; non-stationary SCM channel, 2048 subcarriers, mobile speed 100 km/h

4.2 Carrier Frequency Offset

This scenario is designed to evaluate the performance of CFO estimation. Here, the symbol timing is assumed to be perfect. We also exclude the case where the preamble searching fails. The maximal CFO range is set as ± 15 ppm, and the AWGN channel is considered.

Figure 4-3 shows the Mean Square Error (MSE) performance of the proposed CFO estimator in an AWGN channel. The estimated CFO is already normalized by the subcarrier spacing. Figure 4-4 shows the MSE performances comparison of the proposed CFO estimator and the WOS CFO estimator of [8]. We can see that these two approaches almost have identical performance in the presence of ICFO.

The carrier frequency tolerance for the IEEE802.16 system [2] is 2% of the subcarrier spacing. From the result, we can see that the result meets the requirement even in low SNR environments. The MSE's are all less than 2% as shown in Figure 4-3 and Figure 4-4.

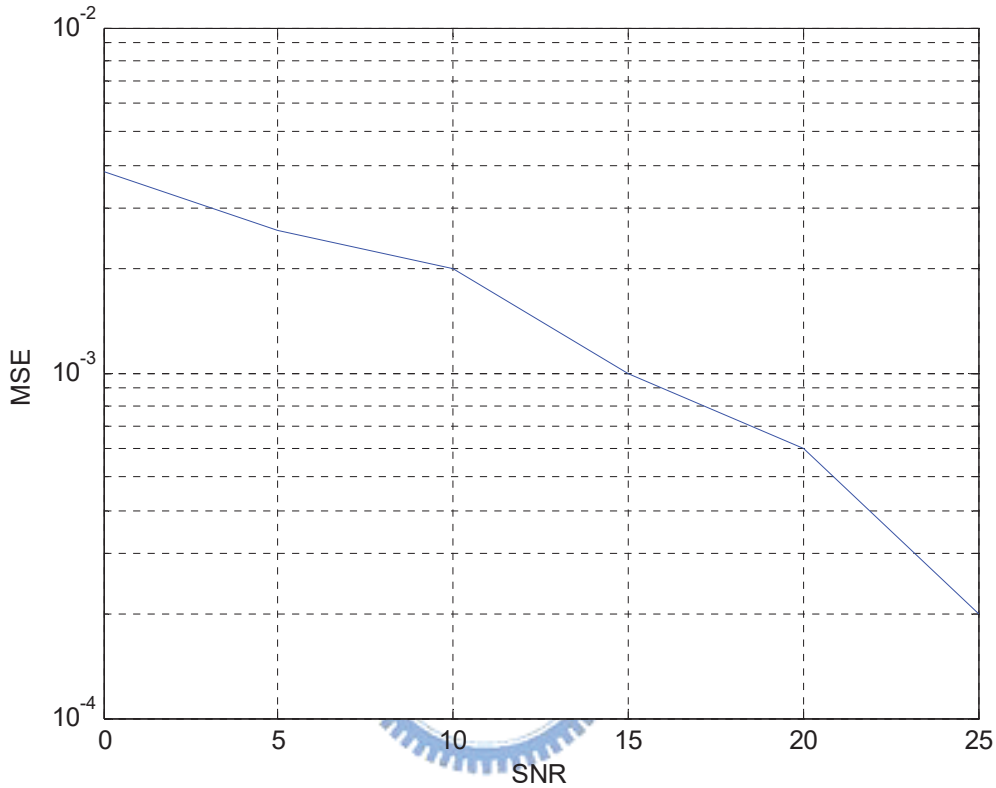

Figure 4-3: Mean square error performance of proposed CFO estimator in an AWGN channel; 2048 subcarriers, CFO ±15 ppm

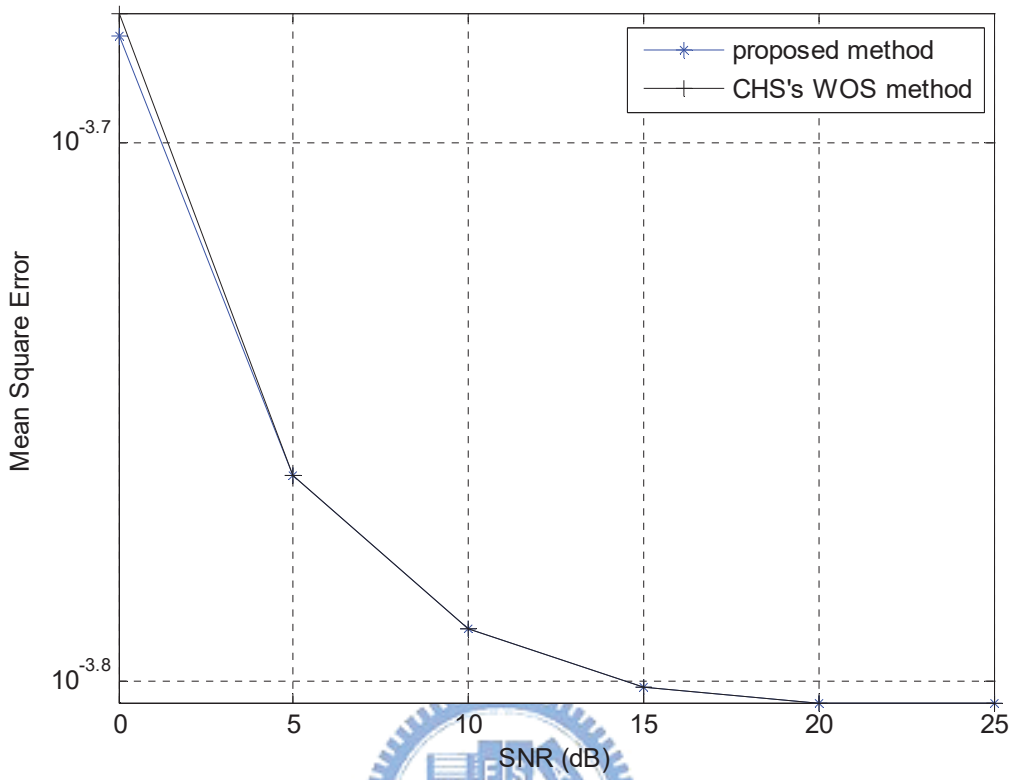

Figure 4-4: Mean Square Error Comparison of the proposed CFO method and the DS-WOS approach [8] in the presence of integer CFO; SCM channel, 2048 subcarriers, ICFO=1 subcarrier spacing

4.3 SFO

Here, the symbol timing is assumed to be perfect and CFO is compensated. Sampling frequency offset is added to simulate the wrong sampling frequency for the receiver.

Figure 4-5 shows the performance comparison for the system with or without SFO. The dash line in Figure 4-5 represents the performance of the system without SFO. The solid line represents the performance of the system with SFO (the SFO is compensated by the channel estimation using pilot signals). CFO is set as 0.5 subcarrier spacing.

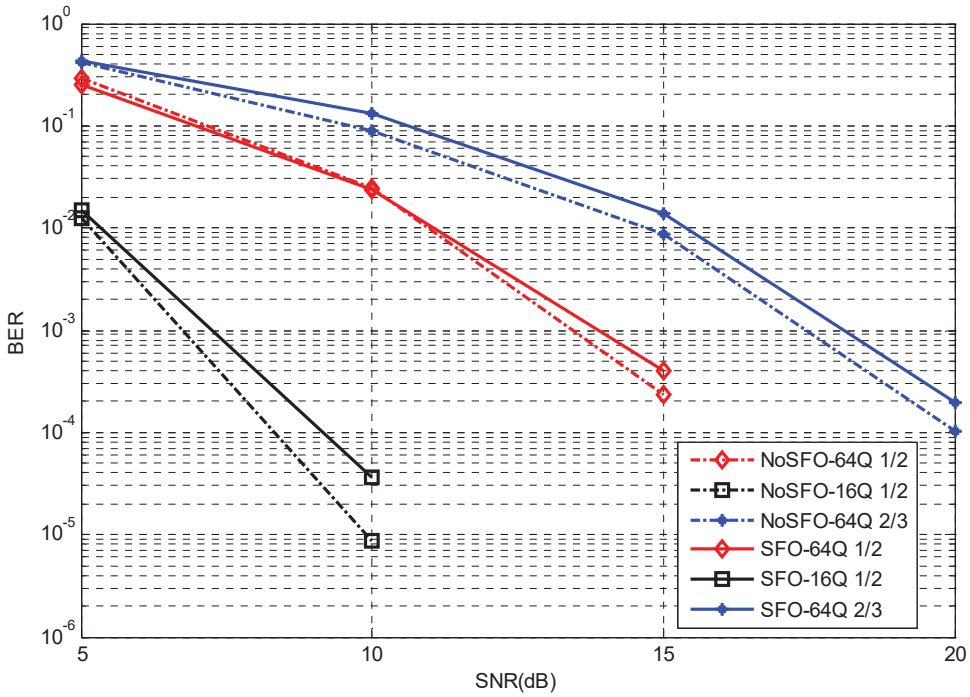

Figure 4-5: Comparison between SFO-less and SFO-compensated system (OFDMA DL)

4.4 Uplink

Since there are no preambles for uplink, most of the synchronization is done during the contention. Hence, for the uplink system, the performance degradation is mainly due to channel estimation.

Figure 4-6 shows the BER performance of the uplink systems under the multipath fading channel in mobile speed of 100km/h and 200km/h. We can see how channel estimation performs in two different mobile speeds. The performance under 100 km/h has slightly better results.

Figure 4-7 shows the BER performance comparison of UL system using known channel and estimated channel. The result of uplink system with estimated channel offers about 1 dB worse than that with the known channel. Figure 4-8 shows the BER performance comparison of the DL and UL system using known channel information. The timing and frequency

synchronization of DL system are all assumed to be perfect in order to meet the presumed synchronization for UL system. Although they share some of common operations, they have different subcarrier allocation and subcarrier randomization. We can see that DL has better performance over UL system due to better subcarrier allocation and subcarrier randomization.

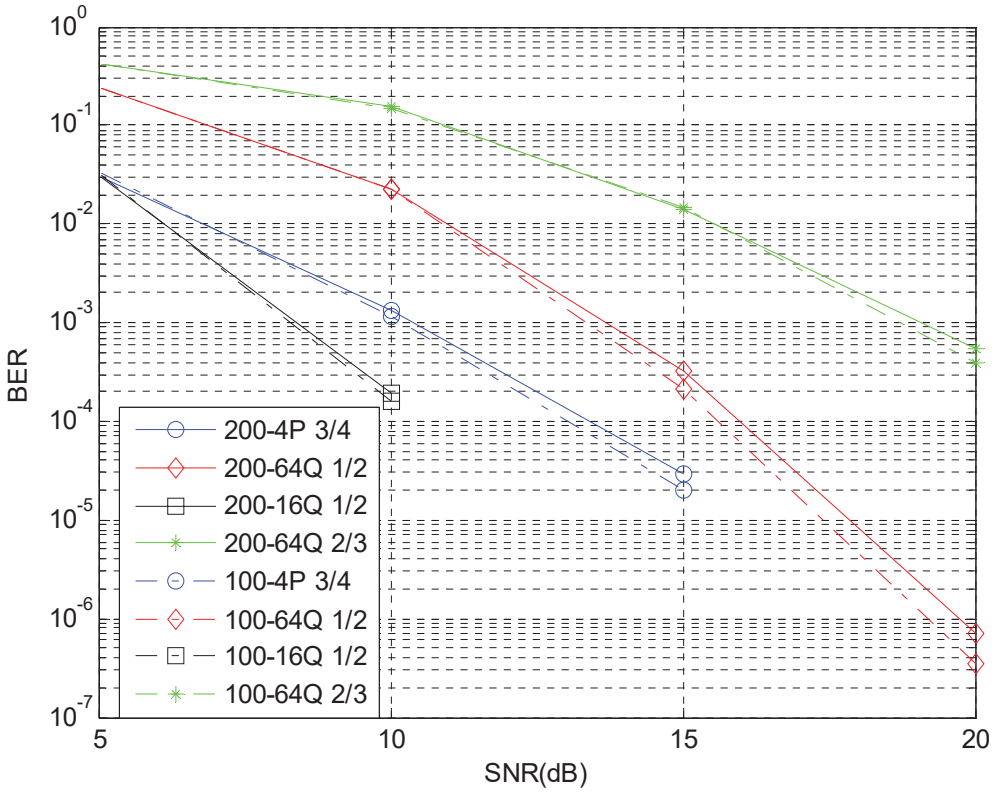

Figure 4-6: BER performance of UL in multipath fading channel (two mobile speeds)

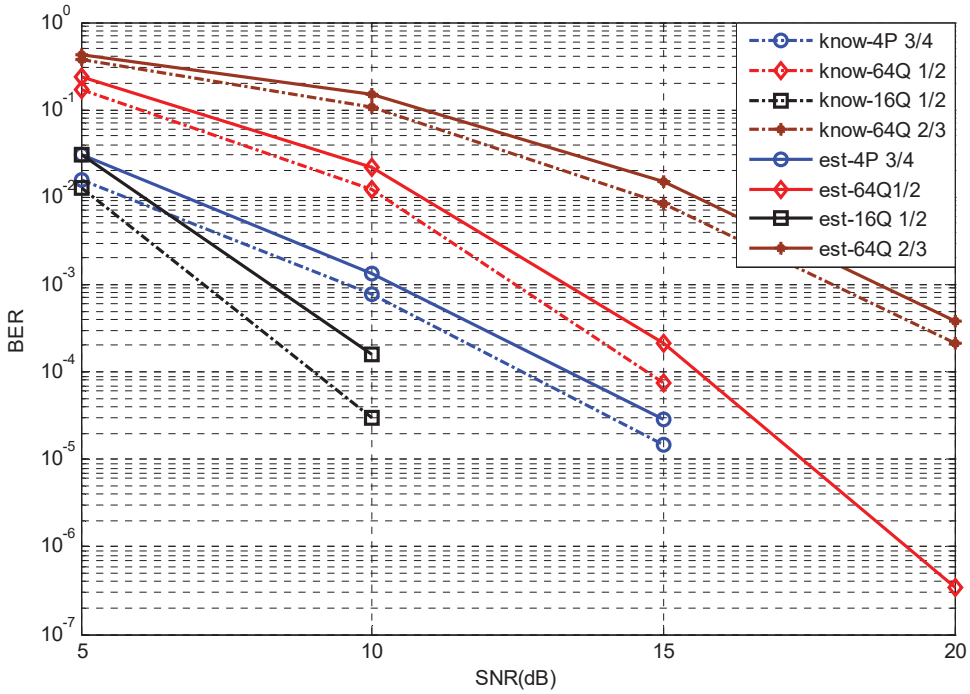

Figure 4-7: BER performance comparison for UL known channel and estimated channel

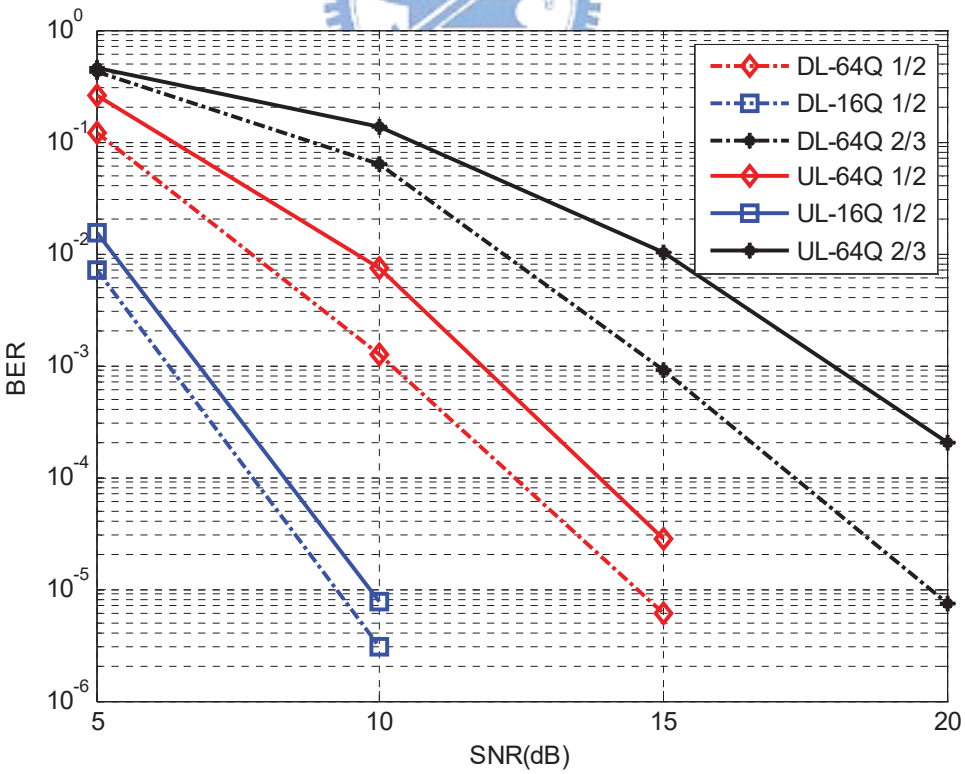

Figure 4-8: BER performance comparison of DL and UL (known channel)

4.5 Downlink using STC

In this simulation, we implement smart antenna technology for DL system. STC involves the transmission of multiple redundant copies of data to compensate for fading and thermal noise in the hope that some of them may arrive at the receiver in a better state than others. In order to show how STC increases the channel capacity, we use two uncorrelated channels for the STC system. One of the channels has more severe multipath fading than the other one. We compare such STC system with the SISO system using worse channel condition in Figure 4-9. Assuming both systems have perfect synchronization except for known channel information. We can see that the STC system do indeed exploit the transmit diversity of the STC to reduce the multipath fading.

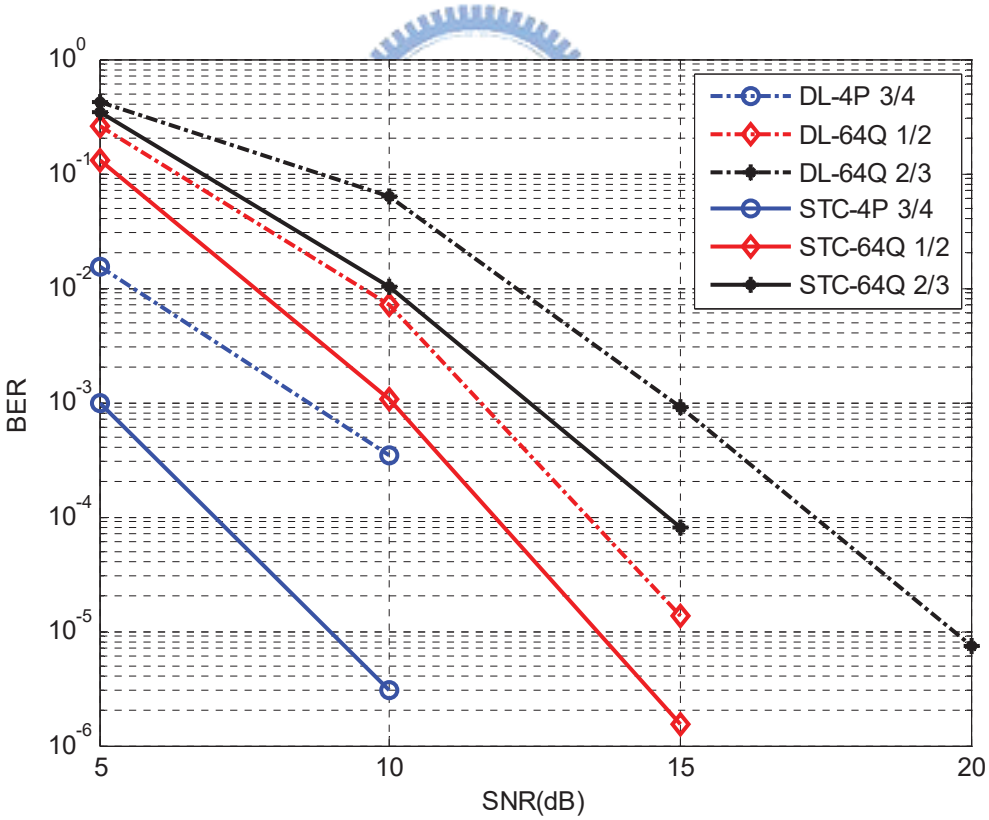

Figure 4-9 : Comparison of SISO DL and STC DL (known channel)

Chapter 5: Conclusions

In this thesis, we propose a low-complexity preamble search algorithm for IEEE802.16 OFDMA systems. The corresponding inner receiver design is also considered. The function of the inner receiver is to cope with the channel effects by performing packet detection, frequency synchronization, preamble search, symbol timing offset estimation, and channel estimation. Compared with the conventional design, our inner receiver can effectively reduce the required computational complexity. With the proposed preamble-search algorithm, we further develop an ICFO estimation algorithm. Computer simulation results show that while the proposed design provides excellent performance, the required computational complexity is low. We also made comparisons with the preamble search proposed by [8].

Apart from the inner receiver design, we also build the platform for both IEEE 802.16 OFDMA uplink and downlink systems. Simulations show that the performance of the downlink system is slightly better, due to the better subcarrier allocation and subcarrier randomization yielded in downlink scenario. For smart antenna technology, the STC exploits transmit diversity when the channel condition is bad. The simulation shows the improvement over SISO system. STC proves to be a simple and effective diversity technique, which is also the goal of our inner receiver design, to combat multipath fading.

Reference

[1] "Air Interface for Fixed Broadband Wireless Access Systems," IEEE Std 802.16-2004.

[2] "Air Interface for Fixed and Mobile Broadband Wireless Access Systems," IEEE Std 802.16e-2005.

[3] WiMAX Forum, "Mobile WiMAX – Part I: A Technical Overview and Performance Evaluation", WiMAX Forum website, August 2006.

[4] WiMAX Forum, "Mobile WiMAX – Part II: A Comparative Analysis", WiMAX Forum website,May 2006.

[5] WiMAX Forum, "Mobile WiMAX: A Performance and Comparative Summary", WiMAX Forum website, September 2006.

[6] Ji Guo-Wei, David W. Lin, "Research in Synchronization Techniques and DSP Implementation for IEEE 802.16e OFDM Uplink and OFDMA Downlink," National Chiao-Tung University, July 2006.

[7] Hsing-Yu Lung, Wen-Rong Wu, "Design and Implementation of IEEE 802.16e OFDMA Baseband Transceiver," National Chiao-Tung University, July 2006.

[8] Hui-Shan Chen, Yu T. Su, "Cell Search and Initial Link Setup for WiMAX Systems," National Chiao-Tung University, July 2006.

[9] Alamouti, S. M., "A simple transmit diversity technique for wireless communications," IEEE Journal on Selected Areas of Communication, vol. 16, pp. 1451-1458, Oct. 1998.

[10] Meng-Han Hsieh and Che-Ho Wei, "A Low-Complexity Frame Synchronization and Frequency Offset Compensation Scheme for OFDM Systems over Fading Channels," IEEE Transactions on Vehicular Technology, Vol. 48, No. 5, September 1999

[11] T.M. Schmidl, D.C. Cox, "Low-Overhead, Low-Complexity Synchronization fir OFDM," IEEE International Conference on Communications, Vol. 3, 1996, pp 1301-1306

[12] Wan-Yi Lin, Wen-Rong Wu, “Channel Estimation and Multiuser Asychronization Interference Mitigation for IEEE 802.16e System,” National Chiao-Tung University, July 2006